

1 **Title:** Computational Saturation Mutagenesis to predict structural consequences of
2 systematic mutations on protein stability and rifampin interactions in the β subunit of
3 RNA polymerase in *Mycobacterium leprae*.

4

5 **Running Title:** *Computational Saturation Mutagenesis–RpoB M. leprae*

6 **Authors:** Sundeep Chaitanya Vedithi^{1*}, Carlos H. M. Rodrigues^{2,3}, Stephanie Portelli^{2,3}, Marcin J.
7 Skwark¹, Madhusmita Das⁴, David B. Ascher^{1,2,3}, Tom L Blundell^{1*} & Sony Malhotra^{1,5}

8 **Affiliations:**

- 9 1. Department of Biochemistry, University of Cambridge, Tennis Court Rd., CB2
10 1GA, UK
11 2. Department of Biochemistry and Molecular Biology, Bio21 Institute, University
12 of Melbourne, Parkville, VIC 3052, Australia.
13 3. Structural Biology and Bioinformatics, Baker Heart and Diabetes Institute,
14 Melbourne, Victoria 3004, Australia
15 4. Molecular Biology Laboratory, Schieffelin Institute of Health-Research and
16 Leprosy Center, Karigiri, Vellore, Tamil Nadu, India 632106.
17 5. Institute of Structural and Molecular Biology, Department of Biological Sciences,
18 Birkbeck College, University of London, London UK, WC1E 7HX

19

20 **Corresponding Authors:**

21

22 **Professor Sir Tom Blundell FRS**

23 Director of Research and
24 Professor Emeritus of Biochemistry

25 **Email :** tlb20@cam.ac.uk

26 Ph: +44 1223 766033

27

28 **Dr Sundeep Chaitanya Vedithi**

29 Research Associate
30 Department of Biochemistry

31 Sanger Building
32 University of Cambridge
33 80 Tennis Ct. Rd., CB2 1GA, UK

34

35 scv26@cam.ac.uk

36 Ph: +44 1223 766033

37

38

39

40

41

42

43

44

45 **ABSTRACT:**

46 In contrast to the situation with tuberculosis, rifampin resistance in leprosy may remain
47 undetected due to the lack of rapid and effective diagnostic methods. A quick and reliable
48 method is essential to determine the impacts of emerging detrimental mutations. The functional
49 consequences of missense mutations within the β -subunit of RNA polymerase in *Mycobacterium*
50 *leprae* (*M. leprae*) contribute to phenotypic rifampin resistance outcomes in leprosy. Here we
51 report *in-silico* saturation mutagenesis of all residues in the β -subunit of RNA polymerase to all
52 other 19 amino acid types and predict their impacts on overall thermodynamic stability, on
53 interactions at subunit interfaces, and on β -subunit-RNA and rifampin affinities using state-of-
54 the-art structure, sequence and normal mode analysis-based methods. A total of 21,394
55 mutations were analysed, and it was noted that mutations in the conserved residues that line
56 the active-site cleft show largely destabilizing effects, resulting in increased relative solvent
57 accessibility and concomitant decrease in depth of the mutant residues. The mutations at
58 residues S437, G459, H451, P489, K884 and H1035 are identified as extremely detrimental as
59 they induce highly destabilizing effects on the overall stability, nucleic acid and rifampin
60 affinities. Destabilizing effects were predicted for all the experimentally identified rifampin-
61 resistant mutations in *M. leprae* indicating that this model can be used as a surveillance tool to
62 monitor emerging detrimental mutations conferring rifampin resistance in leprosy.

63
64 **AUTHOR SUMMARY:**

65
66 Emergence of primary and secondary drug resistance to rifampin in leprosy is a growing
67 concern and poses threat to the leprosy control and elimination measures globally. In the
68 absence of an effective *in-vitro* system to detect and monitor phenotypic rifampin resistance in
69 leprosy, most of the diagnosis relies on detecting mutations in the drug resistance determining
70 regions of the *rpoB* gene that encodes the β subunit of RNA polymerase in *M. leprae*. Few labs in
71 the world perform mouse food pad propagation of *M. leprae* in the presence of drugs (rifampin)
72 to determine growth patterns and confirm resistance, however the duration of these methods
73 lasts from 8 to 12 months making them impractical for diagnosis. Understanding molecular
74 mechanisms of drug resistance is vital to associating mutations to clinical resistance outcomes
75 in leprosy. Here we propose an *in-silico* saturation mutagenesis approach to comprehensively
76 elucidate the structural implications of any mutations that exist or can arise in the β subunit of
77 RNA polymerase in *M. leprae*. Most of the predicted mutations may not occur in *M. leprae* due to
78 fitness costs but the information thus generated by this approach help decipher the impacts of
79 mutations across the structure and conversely enable identification of stable regions in the
80 protein that are least impacted by mutations (mutation coolspots) which can be a choice for
81 small molecule binding and structure guided drug discovery.

82 **INTRODUCTION:**

83

84 Nonsynonymous mutations in genes that encode drug targets in mycobacteria can induce
85 structural and consequent functional changes leading to antimicrobial resistance, the burden of
86 which is rapidly increasing and is a global health concern. Diagnosis of ~600,000 new cases of
87 rifampin-resistant tuberculosis in 2018 suggest that it poses a risk for the concomitant increase
88 in undiagnosed rifampin-resistant leprosy worldwide [1]. *Mycobacterium leprae* (*M. leprae*), the
89 causative bacilli for leprosy, is phylogenetically closest to *Mycobacterium tuberculosis* [2] and
90 developed resistance to rifampicin before the introduction of WHO multi-drug therapy (MDT).
91 Despite the long duration of chemotherapy with MDT (six months in paucibacillary to 12
92 months in multibacillary disease), rifampin-resistant case numbers are less and represent only
93 3-5% of total relapsed leprosy cases reported in 2017 [3]. One of the possible reasons for the
94 low numbers of drug-resistant leprosy cases worldwide is the lack of quick, effective and
95 reliable *in vitro* diagnostic tests for confirming phenotypic resistance. Current methods rely on
96 identifying drug resistance mutations in *rpoB* gene through gene sequencing and/or to test
97 growth patterns of *M. leprae* in response to drugs in an *in vivo* system (footpads of mice), the
98 later technique is both time and labour intensive.

99

100 While mutations within the β -subunit of RNA polymerase contribute to clinical resistance to
101 rifampin, the associated structural changes can complicate the transcription process in bacteria
102 by modulating various complex physiological processes[4], the knowledge of which is essential
103 for novel drug discovery or alternative therapies to treat rifampin resistant strains of *M. leprae*.
104 In the absence of an artificial culture system to propagate and study the molecular mechanisms
105 of resistance, it is exceptionally challenging to define an experimental phenotype for rifampin
106 resistance in leprosy. *M. smegmatis* as a surrogate host with electroporated *M. leprae rpoB* gene
107 has proved a dependable model to study phenotypic effects; however, this technique is limited
108 to biosafety level-2 laboratories that have facilities for gene cloning and sequencing, and cannot
109 be translated to a regular diagnostic setting in leprosy endemic countries[5]. A plausible
110 association between mutations in drug targets and phenotypic resistance outcomes could be
111 established if minimum inhibitory concentrations (MICs) of the drugs are known for the mutant
112 strains. While MICs can be estimated in cultivable species like *M. tuberculosis* and *M. smegmatis*,
113 obtaining growth information from *in vivo* propagation for a slow growing and obligate
114 pathogen like *M. leprae* is often challenging and needs time and resources. *In silico* methods to
115 predict structural implications of mutations will be extremely useful in understanding
116 mechanisms of drug resistance and help prioritise mutations that require experimental
117 validation in leprosy in the absence of a tool for quantitative estimation of the phenotypic
118 resistance outcomes [6].

119

120 Mutations contribute to disruption of protein-ligand and protein-nucleic acid interactions
121 resulting in drug resistance in mycobacterial diseases (Portelli *et al.*, 2018; Karmakar *et al.*,
122 2018). Changes in affinity for the ligand can result from both orthosteric and allosteric
123 mechanism leading to various resistance phenotypes(Vedithi *et al.*, 2018).The β -subunit of RNA
124 Polymerase in *M. leprae* is encoded by the *rpoB* gene (ML1891) whose product is 1178 amino
125 acids in length. The rifampin resistance determining region (RRDR) is located between residue
126 positions 410 and 480. Approximately 40 mutations have been reported in the *rpoB* gene of *M.*
127 *leprae* that cause clinical resistance to rifampin in leprosy[9–11]; however, in tuberculosis,
128 nearly 270 mutations have been reported in the same gene that shares 96% identity with that of
129 *M. leprae* [12]. As the burden of rifampin resistance is very high in *M. tuberculosis* with known
130 and new mutations being reported from different studies[13–17], it is important to monitor the
131 emergence of new rifampin-resistant mutations in *M. leprae*. A comprehensive understanding of
132 the effects of any mutation on the structure of RNA Polymerase (RNAP) is important in the
133 context of monitoring emerging rifampin resistance and its implications on controlling global
134 leprosy incidence.

135

136 In order to decipher the effect of systematic mutations on the stability of the protein structure,
137 protein sub-unit interfaces, nucleic acid and ligand interacting sites, we performed *in-silico*
138 saturation mutagenesis and predicted the stability changes in protein-protein, protein-ligand
139 and protein-nucleic acid affinities. Additionally, we also assessed the impacts of mutations on
140 the secondary structures of the polypeptide chains, on the relative sidechain solvent
141 accessibility, depth and on the residue-occluded packing density. Residue evolutionary
142 conservation scores were determined and compared with the predicted destabilizing effects.
143 Extremely detrimental mutations were selected and analysed for changes in their interatomic
144 interactions that might explain the destabilizing effects. To explore further the vibrational
145 entropy and enthalpic changes of flexible conformations we employed an empirical force field-
146 based method - FoldX[18] , a course-grained normal mode analysis (NMA) based elastic
147 network contact model - ENCoM [19] and a consensus predictor that integrates normal mode
148 approaches with graph-based distance matrix in the mutating residue environment- DynaMut
149 [20]. Finally, fragment hotspots [21] were mapped on the structures to provide information on
150 potential druggable sites whose stability is predicted to be least likely affected by mutations (no
151 mutations in these regions were identified in leprosy). We termed these sites as “Mutation
152 coolspots” which can be explored for novel/alternative small molecule binding and structure-
153 guided drug discovery to treat rifampin-resistant leprosy.

154

155 **MATERIALS & METHODS:**

156

157 **Design:** The key stages in the methodology involve developing of a model based on the known
158 structures of homologues, quality assessment, generating mutation lists and sequential
159 submissions to stability change prediction servers for sequence, structure and vibrational
160 entropic terms (Fig 1A).

161 **Comparative modelling, quality assessment and model refinement:** A model for RNAP
162 holoenzyme of *M. leprae* was built using Modeller 9.21 based using templates from *M.*
163 *tuberculosis* (PDB ID:5UH5 (96% identity, 3.8Å resolution) containing RNAP and nucleic acid
164 scaffold with DNA and three nucleotides of RNA complementary to the template DNA strand and
165 PDB ID: 5UHC (96% identity, 4.0Å resolution) containing all the elements similar to 5UH5 and
166 rifampin) as described earlier by us [4]. The quality of the generated model was assessed using
167 Molprobit [22] and atomic clashes were removed by minimizing the energy of the model by
168 100 steps using Steepest Decent (step size = 0.02 Å) and by 10 steps (step size = 0.02Å) using
169 conjugate gradient algorithms. Energy minimizations were performed using UCSF Chimera[23].
170 The mutant models were generated using Modeller 9.21 [24] (mutate_model.py) and sidechains
171 of the mutants were optimized using ANDANTE [25], a program that uses χ angle conservation
172 criteria to optimize the sidechain rotamers.

173 **Saturated Mutagenesis:** A systematic list of 21,394 mutations for residues from P28 to E1153
174 in the β -subunit (the modelled region) was generated. This list was programmatically submitted
175 to a set of servers that predict protein stability and stability of protein-protein, protein-nucleic
176 acid and protein ligand affinity upon mutations. We also used physics-based potentials to
177 determine impacts of mutations on the RNAP complex in flexible conformations.

178 **Residue Conservation:** Conservation scores for each of the residues in the wild-type model
179 were estimated using CONSURF [26] – a server that uses evolutionary patterns of amino
180 acids/nucleic acids from the multiple sequence alignment and develops a probabilistic
181 framework to calculate evolutionary rates for each residue in the sequence.

182 **Effects of mutations on Protein Stability and Interactions:** The effect of mutations on
183 thermodynamic stability of the protein was analyzed using mCSM [27], SDM [28] and FoldX
184 [29]. For SDM, mutant-protein models were generated using ANDANTE [25], an in-house-
185 developed software that considers conserved χ angle conservation rules while identifying the
186 most probable sidechain rotamers for the mutant residues. The effect of mutations on RNA
187 affinity is assessed using mCSM-NA2[30] on mutant models with nucleic acid scaffold. The
188 holoenzyme complex of RNAP consists of five subunits and the effects of mutations on the
189 protein-protein interfaces (between β and all the other sub-units in RNAP complex) were
190 assessed using mCSM-ppi. Rifampin binds to the β -subunit of RNAP and we analyzed the effects

191 of mutations on the protein-ligand affinity using mCSM-lig [31]. Only residues within 10Å of the
192 interatomic distance to rifampin were analyzed by mCSM-lig.

193 The stability changes were further compared with predictions from other sequence-
194 (PROVEAN[32], I-Mutant 2.0 (Sequence)[33] and structure-based (MAESTRO[34], CUPSAT[35],
195 I-Mutant 2.0 (Structure)) computational tools in order to estimate the reliability of the
196 predictions.

197 **Changes in Vibrational Entropy and Normal Mode Analysis:** In order to determine the
198 effects of the mutations in flexible conformations on protein stability, we used FoldX [18], an
199 empirical force field approach that calculates free energy changes between native and mutant
200 forms of the protein, and an elastic network contact model (ENCoM)[19], which is a coarse
201 grain NMA method that considers the nature of the amino-acids and aids in calculating
202 vibrational entropy changes upon mutations. We also used DynaMut [36], a consensus predictor
203 of protein stability based on the vibrational entropy changes predicted by ENCoM and the
204 stability changes predicted by graph-based signature approach of mCSM.

205 **Conformational Changes:** Conformational changes and their impacts on biophysical properties
206 of the proteins were estimated using SDM [28]. The interatomic distances between each residue
207 and the interface with other subunits in the RNAP holoenzyme, rifampin and nucleic acids in the
208 structure were measured and included in the analysis. Secondary structure switches in mutants,
209 changes in relative solvent accessibility, depth of the residue in Å and residue-occluded packing
210 densities were determined for all the mutations.

211 **Interatomic Interactions:** A few mutations that were experimentally validated elsewhere and
212 are known to be extremely detrimental to stability and ligand interactions were selected and
213 changes in interatomic interactions of the mutating residues were documented using
214 Arpeggio[37], a program that maps the types of interatomic interactions wildtype and mutant
215 residues with the environment based on atom type, interatomic distance and angle constraints.
216 A set of mutations that are not experimentally identified but computationally predicted to have
217 detrimental effects were also chosen from the saturation dataset and a similar analysis was
218 performed. Intermezzo (Bernardo Ochoa Montano & Blundell TL unpublished) was also used for
219 interactive analysis of bonding patterns on Pymol sessions.

220 **Fragment Hotspot Maps:** Fragment hotspot maps [21] aid in locating specific sites on the
221 surface of the protein that are topologically, chemically and entropically favorable for small
222 molecule (fragment) binding. The atomic hotspots on the drug target are explored
223 computationally using donor, acceptor and hydrophobic fragment probes, and introducing a
224 depth criterion to assist in estimating the entropic gain in displacing “unhappy” waters. For
225 ligand-binding proteins, the fragment hotspot maps aid in understanding the pharmacophore

226 characteristics of the interacting regions. We mapped the hotspots on the β -subunit of RNAP and
227 colored the surface with regions that are least impacted by any mutations (mutation coolspots).

228 **RESULTS:**

229 In total 21,394 mutations were generated from 1126 amino acid residues in the β -subunit of
230 RNAP (Supplementary Table-1). The list of experimentally identified mutations and their effects
231 are separately shown in Supplementary Table-2.

232 **Multivariate analysis of free energy changes predicted by different computational tools**
233 **for saturated mutations:** Along with the in-house developed mCSM and SDM tools for
234 prediction of protein stability changes upon saturated mutagenesis of the β -subunit of RNAP, a
235 comparative analysis was performed with other sequence (PROVEAN, I-mutant 2.0 - Sequence),
236 structure- (CUPSAT, I-mutant 2.0-structure, MAESTRO) and NMA-based tools (FOLDX, ENCOM,
237 DynaMut). Average stability changes caused by all possible mutations at each residue position in
238 the β -subunit of RNAP, as predicted by mCSM and SDM, were compared with other structure-
239 based predictors (Supplementary Fig 1) (rifampin-interacting residues are highlighted).
240 Correlation of overall stability predictions performed by mCSM with each of the other tools
241 indicated an “r” value of 0.55 with SDM, 0.61 with MAESTRO, 0.72 with I-mutant 2.0 (Structure)
242 and 0.43 with CUPSAT. Correlations between mCSM, SDM and other sequence and NMA based
243 tools are shown in supplementary figures 2 and 3. The rationale for performing these
244 correlations is to understand how mCSM and SDM being structure-based predictors of stability
245 changes upon mutations, relate to sequence-based methods and vibrational entropy changes in
246 normal mode perturbations.

247 **Experimentally Identified Mutations:** We performed a systematic literature review to list all
248 the mutations reported in the β -subunit of RNAP in *Mycobacterium leprae*. We noted 40
249 mutations at 32 unique residue positions. The reference articles are listed in Supplementary
250 Table -2. As depicted in Fig 1B, 77.5% (31) of the experimentally identified mutations
251 destabilize the β -subunit. Except for A411T and V424G mutations, all the other residues are
252 present in close proximity to rifampin binding sites (Fig 2A) and destabilize rifampin
253 interactions (mCSM-lig).

254 **Residue conservation and protein stability:** The stability changes, predicted after saturation
255 mutagenesis of each residue in the β -subunit, were compared with residue conservation scores.
256 CONSURF scores of less than zero are attributed to conserved residues [26] and scores of zero
257 and above to variable residues (score 3 being maximum and highly variable). The average
258 change in protein stability that was predicted by mCSM for mutations at each residue position
259 ranged from 0.823 to -3.033 kcal/mol and that of SDM varied from 2.167 to -4.36kcal/mol.
260 Residues that line the active center cleft and interact with rifampin and the nucleic acid scaffold

261 are highly conserved, while surface exposed residues have variable conservation scores (Fig 2B).
262 Rifampin-interacting residues between residue positions ~400-500 are highly conserved and
263 87.3% of the saturated mutations in this region destabilize the protein (Supplementary Table 1).
264 The maximum destabilizing effect of mutations at each of these residues varied between -0.311
265 to -4.311kcal/mol(mCSM). The average destabilizing effect predicted by mCSM for all possible
266 mutations at each residue was mapped on to the structure to identify regions are largely
267 impacted by mutations (Fig 2C). Conversely, the residues whose stability is least impacted by all
268 possible mutations are colored in blue to identify “mutation coolspots” that are potentially areas
269 of choice for targeting with small molecules in drug discovery (Fig 2D).

270 As part of the RNAP holoenzyme complex, the β -subunit interacts with other subunits and has
271 large interfacial regions. The impact of mutations on the stability of these interfaces was
272 measured using mCSM-ppi. It was noted that the maximum destabilizing effect by any mutation
273 at a particular residue in the interface between β and β' subunits has an affinity change that
274 ranged from -0.021 to -5.108 kcal/mol (-5.108kcal/mol was noted for mutation W1074R which
275 is not reported experimentally in rifampin resistant leprosy cases). The interfacial region and
276 the stability changes are mapped on the structure (Fig 3A and B).

277 **Relative sidechain solvent accessibility (RSA), depth, residue-occluded packing density**
278 **and protein stability:** The difference in relative solvent accessibility between wild type and the
279 mutant residue for all the mutations were calculated using SDM. While analyzing the maximum
280 destabilizing mutations among all the possible mutations at each residue position, it was noted
281 that maximum destabilizing mutants at 751 residue positions (66.79%) show increases in RSA.
282 The maximum destabilizing mutants at rest of the 375 residue positions indicated a decrease in
283 RSA. Among the maximum destabilizing mutants at 751 residue positions which showed an
284 increase in RSA, 551 were hydrophobic and 121 substitutions within 551 were from
285 polar/charged (wildtype) to hydrophobic residues (mutants). As mutant hydrophobic residues
286 with increased solvent accessibility often destabilize the protein [38], the destabilizing effects of
287 these mutations ranged from -1.021 to -4.311 kcal/mol. Additionally, these substitutions
288 resulted in a decrease in residue-depth [28] (ranging from 0.01 Å to 1.83Å), which is
289 concomitant with the increase in solvent accessibility. These changes in RSA and depth at the
290 rifampin-binding site are depicted in Fig 4A & B.

291 From the maximum destabilizing mutations at all the 1126 positions, mutations at 586
292 (52.04%) residue positions resulted in increase in depth that ranged from 0.01 to 2.46Å.
293 Mutants were generated using ANDANTE a program that follows χ angle conservation rules to
294 place the sidechains of the mutant residue without any steric clashes. This is followed by energy
295 minimization. Hence the change in depth is attributed to the buriedness of the residue and not
296 just the natural change from a larger to a smaller amino acid. The decrease in depth in the

297 remaining 540 (47.95%) residues ranged from 0.1 to 3.02Å. Similarly, the residue-occluded
298 packing density [28] increased at 539 residue positions (47.86%). These changes in RSA and
299 depth are mapped as attributes on to the structure of the β -subunit of RNAP and it was noted
300 that most of the residues that line the active center cleft have increases in RSA upon mutation.
301 Decrease in depth was noted in residues at the rifampin-binding pocket and at the subunit
302 interfaces (Fig 5A & B).

303 **Substitutions to aspartate predominate mutations that destabilize the β subunit-RNA** 304 **affinity in RNAP:**

305 The effects of mutations on β subunit-RNA affinity was estimated using mCSM-NA2.
306 Substitutions to aspartate residues were most common among mutations that highly destabilize
307 β subunit-RNA interactions in RNAP. The mutant aspartate residues induced π - π interactions
308 with the nucleotides in RNA either by stacking or by nucleotide-edge T-shaped and amino-edge
309 T-shaped interactions. Aspartate being an acyclic π -containing amino acid, readily forms
310 nucleotide (edge) amino (edge) or nucleotide (face) and amino-acid (edge) interactions. This
311 ability of acyclic amino acids like arginine, glutamic acid and aspartic acid to form a variety of
312 charged- π interactions with nucleotides in mutants may impact the orientation of RNA
313 molecules in active center cleft of RNAP leading to loss or gain in function. Approximately, 93%
314 of the highly destabilizing mutations at each RNA-interacting residue are substitutions to
315 aspartate. Mutations to glutamate were also noted in 6.83% and additionally one each of
316 methionine, proline and threonine mutations indicated highly destabilizing effects.

317 **Substitutions to arginine predominate mutations that destabilize β subunit-rifampin** 318 **affinity:** Systematic mutations in the set of 70 residues that lie 10 Å from the rifampin binding 319 site reveal that highly destabilizing mutations are primarily arginine and glutamate 320 substitutions (mCSM-lig). In the binding site R173, R454, R465 and R613 form hydrogen bonds 321 and a network of interatomic interactions with rifampin that stabilize the molecule in the 322 binding site [4]. Introduction of additional arginine residues by mutations may influence the 323 stability and orientation of rifampin in the binding site. In predicted mutations S437R and 324 G456R, arginine forms an intricate network of interactions with surrounding aromatic amino 325 acids changing the shape of the binding pocket and leading to a loss in rifampin interactions 326 (rifampin retains only two polar contacts with Q438 and F439 where as wild-type has around 327 five hydrogen bonds). The effects of mutations on RNA and rifampin affinity as predicted by 328 mCSM-NA2 and mCSM-lig were mapped on to the structure (Fig 6A & B).

329 **Detrimental Mutations:** Six residues were chosen based on the following characteristics and 330 the structural effects of systematic mutations at each residue position were analyzed (Table-1) 331

- 332 • Mutations that highly destabilize rifampin binding (at wildtype S437 & G459)
- 333 • Experimentally identified and validated mutations that highly destabilize rifampin
- 334 binding ((at wildtype H451 & P489)[9,10].
- 335 • Predicted extremely detrimental mutations for protein stability, and protein-protein and
- 336 protein-nucleic affinities (at wildtype K884 & H1035).

337 **Table 1:** Detrimental mutations and their corresponding stability changes that influence

338 holoenzyme assembly, rifampin and RNA interactions.

Method	Wild-Type Residue	Residue Position	Average Stability Effect	Maximum Stabilizing Effect	Mutant Residue	Maximum Destabilizing Effect	Mutant Residue
mCSM-Stability	S	437	-0.795	-0.072	L	-1.701	H
	H	451	-1.214	-0.104	Y	-1.898	S
	G	459	-0.713	-0.381	V	-1.201	W
	P	489	-1.135	-0.507	R	-1.771	G
	K	884	-1.227	-0.190	L	-2.298	S
	H	1035	-0.419	0.600	Y	-1.421	G
mCSM-PPI	S	437	-0.254	0.395	H	-0.820	R
	H	451	-0.652	-0.050	S	-1.451	M
	G	459	-0.397	0.237	H	-1.042	R
	P	489	-0.738	-0.138	W	-1.372	R
	K	884	-0.105	0.160	D	-0.685	R
	H	1035	-0.754	0.115	W	-1.726	R
mCSM-NA	S	437	-1.538	4.922	W	-3.857	D
	H	451	-1.300	5.147	W	-3.632	D
	G	459	2.289	8.556	W	-0.221	D
	P	489	1.926	8.195	W	-0.582	D
	K	884	0.221	6.647	W	-2.130	D
	H	1035	0.847	7.295	W	-1.484	D
mCSM-Lig	S	437	-0.646	-0.484	L	-1.062	R
	H	451	-0.510	-0.076	W	-0.777	E
	G	459	-0.981	-0.715	A	-1.236	R
	P	489	-0.598	-0.254	L	-0.917	R
	K	884	-0.156	-0.368	D	-0.925	R
	H	1035	-0.121	0.097	V	-0.501	E
SDM	S	437	0.087	2.320	V	-1.900	P
	H	451	-0.756	1.290	L	-2.800	G
	G	459	-2.842	-1.780	V	-3.800	P
	P	489	-0.432	1.440	Y	-1.070	E
	K	884	0.108	1.270	V	-1.820	P
	H	1035	-0.200	0.590	V	-1.410	P
MAESTRO	S	437	-0.21	-0.14	K	0.24	F
	H	451	-0.12	-0.05	G	0.22	R
	G	459	-0.23	-0.17	S	0.33	W
	P	489	-0.26	-0.22	H	0.31	M
	K	884	-0.20	-0.14	G	0.25	M
	H	1035	-0.27	-0.25	P	0.31	Y
CUPSAT	S	437	2.70	7.98	I	-1.12	G
	H	451	2.01	6.92	W	-3.25	K
	G	459	-2.51	5.00	K	-5.53	C
	P	489	-2.76	-0.84	A	-5.47	M
	K	884	-2.99	3.42	I	-8.03	H
	H	1035	-1.07	2.15	C	-3.23	Y
Imutant 2.0 Structure	S	437	4.05	9.00	A	1.00	F
	H	451	6.00	8.00	G	3.00	L
	G	459	6.63	9.00	N	3.00	I
	P	489	7.11	9.00	G	3.00	L
	K	884	6.42	9.00	G	2.00	M
	H	1035	4.63	8.00	G	2.00	L

PROVEAN	S	437	-4.79	-3.00	A	-7.00	W
	H	451	-8.66	-5.73	Y	-10.37	C
	G	459	-8.10	-6.00	A	-10.00	L
	P	489	-9.04	-7.99	A	-10.99	F
	K	884	-5.97	-2.91	R	-7.75	C
	H	1035	-8.98	-5.79	Y	-10.61	C
Imutant 2.0 Sequence	S	437	4.47	7.00	F	0.00	H
	H	451	3.21	7.00	P	0.00	F
	G	459	3.53	7.00	H	0.00	A
	P	489	6.89	9.00	G	5.00	L
	K	884	3.53	8.00	V	0.00	G
	H	1035	2.95	6.00	G	0.00	V
FOldX4	S	437	2.79	-1.44	I	12.39	R
	H	451	1.78	-0.74	L	4.39	W
	G	459	9.14	3.96	A	20.76	H
	P	489	3.04	2.11	N	4.79	R
	K	884	1.06	-2.12	Y	9.77	L
	H	1035	0.77	-1.47	P	5.69	Y
ENCoM	S	437	-0.44	0.48	G	-1.50	W
	H	451	0.34	0.97	G	-0.46	W
	G	459	-0.91	-0.29	A	-1.55	W
	P	489	-0.16	0.14	G	-0.82	F
	K	884	0.18	0.96	G	-0.60	W
	H	1035	0.19	0.73	G	-0.26	W
DynaMut	S	437	2.87	6.99	L	-2.08	G
	H	451	-0.74	2.17	Y	-3.43	T
	G	459	1.93	3.29	N	-0.25	S
	P	489	0.94	3.26	F	-0.72	S
	K	884	0.14	3.69	W	-1.87	E
	H	1035	0.21	2.38	W	-2.29	G

339

340 **Detrimental mutations in the rifampin binding site:** We have noted that any mutation at
341 rifampin-interacting residues S437, H451, R454, S456, L458, G459, R465, P489, P492 and N493
342 destabilize protein ligand affinity (mCSM-lig). Of these we have chosen wild-type residues H451
343 and P489, which are experimentally identified mutations, and wild-type residues S437 and
344 G459, which are computationally predicted (only one mutation was experimentally identified at
345 residue position S437L as reported by us earlier [4], and this has destabilizing effects on the
346 overall stability and affinity to rifampin).

347

348 **S437:** Serine at position 437 in the wild-type structure forms mainchain and sidechain
349 hydrogen bond interactions with S434, G432 and R173. The residue has a network of proximal
350 polar interactions and hence stabilizes the rifampin-binding pocket. It was noted that any
351 mutation at this position reduces rifampin affinity (mCSM-lig) and stability of the β subunit
352 (mCSM) (Supplementary-Table 1) (Fig 7A). The maximum destabilizing effect was noted for
353 substitution to histidine (-1.701 kcal/mol (mCSM)) where it forms hydrogen bond interactions
354 with S434 and Q438, aromatic interactions with F431, and a network of ring-ring and π
355 interactions with the surrounding residues which might largely effect the shape of the binding
356 pocket (Fig 7B). Substitution with leucine causes a minimal destabilizing effect (-0.072 kcal/mol
357 (mCSM)) and stability effects of all the other amino acid substitutions range from -0.072 to -
358 1.701 kcal/mol(mCSM).

359

360 S437 is located at 3.3 Å from the interface of β and β' subunits. Arginine substitution
361 destabilized the interface with the predicted interface stability change of -0.820 kcal/mol
362 (mCSM-ppi). In the wild-type structure, S437 is located 11.9 Å from the closest nucleic acid
363 molecule but is present on the helix that interacts with both DNA and transcribing RNA in the
364 active center cleft. An aspartate substitution destabilizes the protein-RNA interaction with
365 predicted affinity change of -3.857 kcal/mol (mCSM-NA2). S437 is located 4.0 Å from rifampin
366 and forms proximal interactions with rifampin. However, S437 forms hydrogen bond
367 interactions with S434 and R173 that are important for the attachment of rifampin to the
368 binding pocket. The S437R mutation disrupts the hydrogen bond interactions with S434 and
369 R173 which in-turn impact stability of rifampin in the binding pocket (-1.062 kcal/mol (mCSM-
370 lig)).

371

372 **G459:** Glycine at position 459 forms hydrogen bonds with Q435, L458 and G462, and carbonyl
373 interactions with the P460. G459 is present 4.6 Å away from rifampin and is involved in
374 hydrogen bonds with residues that interact with rifampin (Fig 7C). A tryptophan substitution
375 largely destabilizes the binding pocket by the incorporation of hydrophobic and π interactions
376 with the surrounding residues. It forms side-chain hydrophobic interactions with L436, L384
377 and F430. It also forms a ring-ring interaction with F430, an atom-ring interaction with L384
378 and intergroup interactions with Q178 and Q388. It forms multiple hydrogen bonds with the
379 surrounding residues, which may impact the orientation of the binding pocket and destabilize
380 the protein (Fig 7D).

381

382 **Experimental Mutations that highly destabilize rifampin binding:** From the 40 mutations
383 that are reported from different rifampin-resistant leprosy clinical isolates, we have chosen two
384 residues where mutations are extremely detrimental to protein stability, protein ligand affinity,
385 protein nucleic affinity and protein subunit interfaces. Substitutions at H451 and P489 were
386 studied in detail.

387

388 **H451:** H451 in the wild-type structure lies 3.7Å from rifampin and 4.1Å from the interface. This
389 residue forms cation - π interactions with guanidinium group of R454, which in turn forms polar
390 interactions with rifampin (Fig 8A). Additionally, H451 makes two hydrogen bonds with
391 mainchain amino group of R454 and oxygen atom of S447. Mutations at this residue site largely
392 impact the stability and ligand binding. Substitution to serine induced a change in stability of
393 the protein with a decrease in Gibbs free energy of -1.898 kcal/mol and a network of π
394 interactions that are present in the native structure were lost in the mutant (Fig 8B).

395 Methionine substitution destabilizes β - β' subunit interface and leads to a change in free energy
396 of -1.451 Kcal/mol. Methionine forms carbonyl interactions with K452 and T450, a hydrophobic
397 interaction with Q438 and weak hydrogen bond interactions with rifampin. Although histidine
398 or methionine do not directly interact with the residues of the β' subunit, the changes in the
399 network of π -interactions coupled with the addition of hydrophobic interactions with proximal
400 residues in the interface may change their binding patterns leading to destabilization of the
401 interface.

402 Substitution with glutamic acid induces a destabilizing effect on the β subunit-rifampin
403 interaction. E451 forms weak hydrogen bond, carbonyl and proximal hydrophobic interaction
404 but does not form any bonds with rifampin, unlike the wild-type residue that forms proximal
405 hydrogen bonds with rifampin.

406 **P489:** Proline at position 489 is present in a loop which is in close proximity to rifampin and
407 forms hydrophobic interaction with rifampin and weak hydrogen bond interactions with T488
408 and Q490 (Fig 8C). Mutations at the position 489 were reported in rifampin-resistant leprosy
409 patients from Thailand [9]. Glycine substitution destabilizes the protein (-1.771kcal/mol)
410 leading to a loss of hydrophobic interaction with rifampin. Weak hydrogen bond and carbonyl
411 interactions, however, were retained in the mutant model (Fig 8D). Arginine substitution
412 destabilizes interface and rifampin affinities, with predicted stability changes of -1.372 and -
413 0.917 kcal/mol respectively. FoldX predicted a large change in stability of 4.79 kcal/mol for
414 difference between mutant and wild types, which is highly destabilizing. FoldX optimizes the
415 sidechains and moves the structure to a lowest energy state (usually represented as a negative
416 value) and hence the difference between two negative energy values of wild and mutant is
417 destabilizing.

418 **Extremely Detrimental Mutations:** Mutations at residues positions K884 and H1035 were
419 considered to be extremely detrimental. These residues lie in close proximity to the interface,
420 nucleic acids and rifampin. Substitutions at these sites destabilize protomer, protein-protein
421 interfaces (both the residues reside at the subunit interface), protein-nucleic acid and protein-
422 ligand affinities. Both empirical (FoldX) and knowledge based (mCSM and SDM) methods
423 predicted destabilizing effects.

424 **K884:** K884 is located 3.2 Å from the interface, 3.3 Å from the nucleic acid and 8.6Å from
425 rifampin. Lysine forms mainchain hydrogen bonds with L1033 and proximal hydrophobic
426 interactions with H1035 and V894. It also forms a cation - π interactions with H1035 and most
427 importantly a sidechain proximal hydrogen bond with the sugar phosphate group of guanine
428 (second) nucleotide in the RNA transcript. This interaction is critical for maintaining the RNA
429 interaction with rifampin in order to induce steric clash on the adjacent nucleotide and halt

430 transcription (Fig 9A). Serine substitution at this site results in the loss of these vital
431 interactions. S884 forms weak van der Waals interactions with D883 and L885 and hydrogen
432 bonds with L1033 and H1035. Interactions with RNA backbone are lost in the mutant (Fig 9B).
433 The mutant is destabilized with a predicted stability change of -2.298 kcal/mol.

434 Aspartate substitution at this site destabilizes RNA affinity with a change of -2.130 kcal/mol and
435 the mutant residue forms hydrogen bonds with L1033 and H1035, and hydrophobic interactions
436 with V894.

437 **H1035:** Histidine at position 1035 is located 3.5 Å from the interface and RNA, and 8.8Å away
438 from rifampin. It forms a network of π interactions with the surrounding residues. The ring-ring
439 π interactions with the fused pyrimidine-imidazole ring of guanine in the first nucleotide of RNA
440 transcript is vital to the orientation of RNA transcript in the active center cleft (Fig 9C). These
441 interactions are lost in mutations especially with non-aromatic amino acids. It was also noted
442 that aspartate substitution largely destabilizes β subunit -rifampin affinity (Fig 9D).

443 **Impact of Mutations on Flexible conformations:** The stability changes between the wildtype
444 and each mutant in lowest energy conformation were calculated by FoldX and have a Pearson's
445 correlation coefficient ("r" value) of 0.38 with other predictors mCSM and SDM. Although FoldX
446 does not probe backbone conformational changes, it optimizes the sidechain rotamers of the
447 mutant residues to attain a low energy state and calculates the change in free energy between
448 the states. We further sampled the fully flexible conformers of the β subunit and estimated
449 changes in vibrational entropy ΔS and protein stability using ENCoM. A linear combination of
450 vibrational entropy ΔS by ENCoM and enthalpy changes by FoldX was used to calculate stability
451 changes. ENCoM predicted highly destabilizing mutations in the rifampin binding and RNA
452 interacting sites in the active center cleft of the holoenzyme. DynaMut predictions correlated
453 with ENCoM values at an r value of 0.56. The average change in stability predicted by ENCoM
454 and DynaMut for any mutation at each residue in the β subunit was mapped on the structure
455 (Fig 10A and B).

456 **Stability changes and fragment hotspot maps:** Hotspots were mapped on the structure and
457 colored with maximum destabilizing effects caused by any mutations at each residue site. The
458 regions of the β subunit that are least impacted by mutations (mutation coolspots) are overlaid
459 with fragment hotspots. The site B (Fig 11), which is in close proximity to the RNA binding
460 region and is a pocket at the β - β' subunit interface, is least impacted by mutations and has a
461 hotspot at the contouring score of 17 with donor, apolar and acceptor regions [21]. Secondly, the
462 site A, although located away from the catalytic core of the enzyme, is present in the path of
463 entry/exit point for template DNA into the holoenzyme complex and a small molecule
464 interaction at this site can potentially impact template DNA interactions or induce

465 conformational change in the crab-claw-shaped β subunit leading to disruption in the
466 holoenzyme assembly.

467 **DISCUSSION:**

468 In the absence of a rapid and an effective laboratory-based diagnostic tool for determining drug
469 resistance in leprosy, identification of mutations known to confer resistance to individual drugs
470 in multidrug therapy remains an appropriate approach for diagnosing drug resistance.
471 Associations between mutations in drug targets and clinical resistance to individual drugs in
472 MDT are often validated by mouse-footpad experiments in which, resistant strains (with known
473 mutations) are propagated in the hind footpads of mice (cross-bred albino) in the presence of
474 drugs under study [4]. Rifampin resistance is widespread in tuberculosis with annual global
475 incidence of ~600,000 cases and since the molecular mechanisms of drug action are similar in
476 both tuberculosis and leprosy, it is expected that rifampin-resistant strains of *M. leprae* may also
477 exist in numbers much higher than those reported through various epidemiological studies[10].
478 Owing to high percentage identity of the β subunit of RNAP of *M. leprae* with that of *M.*
479 *tuberculosis*, identical mutations that are experimentally proven to confer rifampin resistance in
480 tuberculosis, are considered as likely drug-resistant mutations in leprosy. The experimentally
481 known mutations in *M. leprae* were those identified by DNA sequencing of *rpoB* gene (derived
482 from skin tissues DNA of relapsed/drug resistant leprosy patients) and published in different
483 studies (references for each mutation are listed in Supplementary Table-2). Most of these were
484 validated in either mouse foot-pad experiments or by using surrogate genetic hosts. Any new
485 mutations that emerge will need experimental validation using mouse footpad /other
486 experimental methods, which are time consuming, posing the need for effective alternative
487 solutions to decipher the possible impacts of the mutations on drug-resistance outcomes [39].

488 Around 40 different rifampin-resistance mutations were noted in *M. leprae* from clinical isolates
489 around the world using amplicon sequencing of rifampin resistance determining
490 region(RRDR)[10]. All of these mutations decrease the stability of rifampin binding to the β
491 subunit of RNAP (Supplementary Table-1) and the mutant strains exhibited normal grown
492 patterns in the mouse footpads when administered with rifampin in doses equivalent to WHO
493 regimen of MB MDT [40]. This indicates that mutations structurally and functionally impact
494 rifampin interactions and the concomitant resistance.

495 Thermodynamic stability of the proteins essentially influences their function and is largely
496 dependent on the sequence. Missense mutations that lead to amino acid substitutions often
497 impact protein stability, shifting it towards either a stabilized or a destabilized state [7].
498 Experimental measurements of stability changes in proteins are often challenging especially
499 with large and complex protein machineries like RNAP. However, mutations within each subunit

500 of the RNAP complex, and primarily the rifampin binding β subunit, have clinical implications
501 and influence rifampin-resistance outcomes in mycobacterial diseases[41]. The performance of
502 various structural, sequence and NMA based predictors for predicting protein stability changes
503 upon mutations vary largely in terms of their accuracy and bias[42], but offer a quick and a
504 helpful alternative to understanding the association between mutations and resistance
505 phenotypes[6].

506 Given the absence of a rapid and experimentally validated system to read the impact of
507 mutations in the β -subunit of RNAP in *M. leprae* with clinical rifampin resistance outcomes in
508 leprosy, we conducted computational saturation mutagenesis to determine regions on the β
509 subunit that impact the overall stability, protein-subunit interfaces, protein-nucleic and protein-
510 ligand affinities. Being a part of the complex transcriptional machinery in the mycobacterial cell,
511 the compositional and conformational stability of the β -subunit is crucial to binding of DNA
512 template and synthesis of complementary RNA transcript in the active center cleft of the
513 holoenzyme[43,44]. As rifampin blocks the growing RNA transcript through steric occlusion, its
514 binding and orientation in the binding pocket are vital to its function [43]. Mutations within the
515 RRDR impact rifampin interactions and overall stability of the subunit. As noted from Table 1, all
516 the experimentally identified *rpoB* gene mutations from *M. leprae* indicated a destabilizing effect
517 on the protein-ligand affinity. Owing to the robustness of these predictions, we employed an *in-*
518 *silico* saturation mutagenesis model to understand the impacts of systematic mutations at each
519 residue site of the subunit.

520 The destabilizing mutations are given preference over mutations that are silent or have minimal
521 effects on the stability. This is to explore and understand the possible structural and functional
522 implications of emerging detrimental mutations (reported or new) that can influence rifampin
523 resistance outcomes in leprosy. We used different structural, sequence and NMA based tools to
524 identify and compare the predictions. mCSM stability predictions had better correlations with
525 the other predictors (SDM ($r=0.55$), MAESTRO ($r=0.61$), Imutant 2.0 Structure ($r=0.72$), CUPSAT
526 ($r=0.43$), Imutant 2.0 Sequence ($r=0.62$) and Dynamut ($r = 0.61$)).

527 Protocols (Computational Saturation Mutagenesis (CoSM))[45] that use molecular dynamic
528 equilibration, sidechain flips and energy minimization to improve side conformations in
529 mutants enable prediction of stability changes with better accuracy and correlation with the
530 experimentally deciphered stability changes ($r=0.9$). However, these protocols are
531 computationally intensive and require high performance computing systems and time. CoSM
532 had a similar performance to FoldX, which was used in the current study. Given the large sample,
533 size molecular dynamic equilibration of sidechain rotamers is beyond the scope of this study.

534 In conclusion, we have deciphered the predicted effects of all possible mutations in the β
535 subunit of RNAP of *M. leprae* using computational saturation mutagenesis model, probing
536 structural, sequence driven and dynamic changes that impact overall stability of the protein,
537 RNA and rifampin affinities. The predicted impacts were mapped onto the structures and highly
538 detrimental mutations are further analyzed for their changes in interatomic interactions. Due to
539 the lack of adequate experimental data on stability changes in β subunit of RNAP upon
540 mutations, we have limited information on the accuracy of the predictions, however, all the
541 prediction tools used in the study are well tested and validated software which are proven to
542 perform with reasonable accuracy and minimal bias on various relevant mutational datasets
543 [34]. To date there were no studies describing the phenotypic resistance/susceptibility
544 outcomes in strains with compensatory mutations in RNAP. Further studies on saturation
545 mutagenesis of the entire RNAP holoenzyme complex may provide comprehensive information
546 on the effects of co-evolving and compensatory mutations in other subunits on rifampin binding
547 and function.

548 **ACKNOWLEDGEMENTS:**

549 Authors would like to thank the rest of the computational biology team at Department of
550 Biochemistry, University of Cambridge for their overarching support and guidance in the data
551 collection and analysis. SCV was supported by American Leprosy Missions Grant (G88726), MJS
552 was supported by a grant from Foundation Botnar working to support children with cystic
553 fibrosis (Project 6063), CHMR and SP were supported by Australian Government Research
554 Training Program Scholarships, DBA was funded by a Newton Fund RCUK-CONFAP Grant
555 awarded by The Medical Research Council and Fundação de Amparo à Pesquisa do Estado de
556 Minas Gerais (MR/M026302/1) and by the Wellcome Trust Programme Grant (200814/Z/16/Z)
557 and supported in part by the Victorian Government's OIS Program. TLB was supported by the
558 Wellcome Trust Programme Grant (200814/Z/16/Z) and SM was supported by the MRC DBT
559 Grant (RG78439).

560 **COMPETING INTERESTS:**

561 The authors declare no competing interests.

562 **REFERENCES:**

- 563 1. World Health Organization. Global tuberculosis report 2018 [Internet]. World Health
564 Organization; 2018. Available: <http://apps.who.int/iris/handle/10665/274453>
- 565 2. Han XY, Sizer KC, Thompson EJ, Kabanja J, Li J, Hu P, et al. Comparative Sequence Analysis
566 of *Mycobacterium leprae* and the New Leprosy-Causing *Mycobacterium lepromatosis*. *J*
567 *Bacteriol.* 2009;191: 6067–6074. doi:10.1128/JB.00762-09

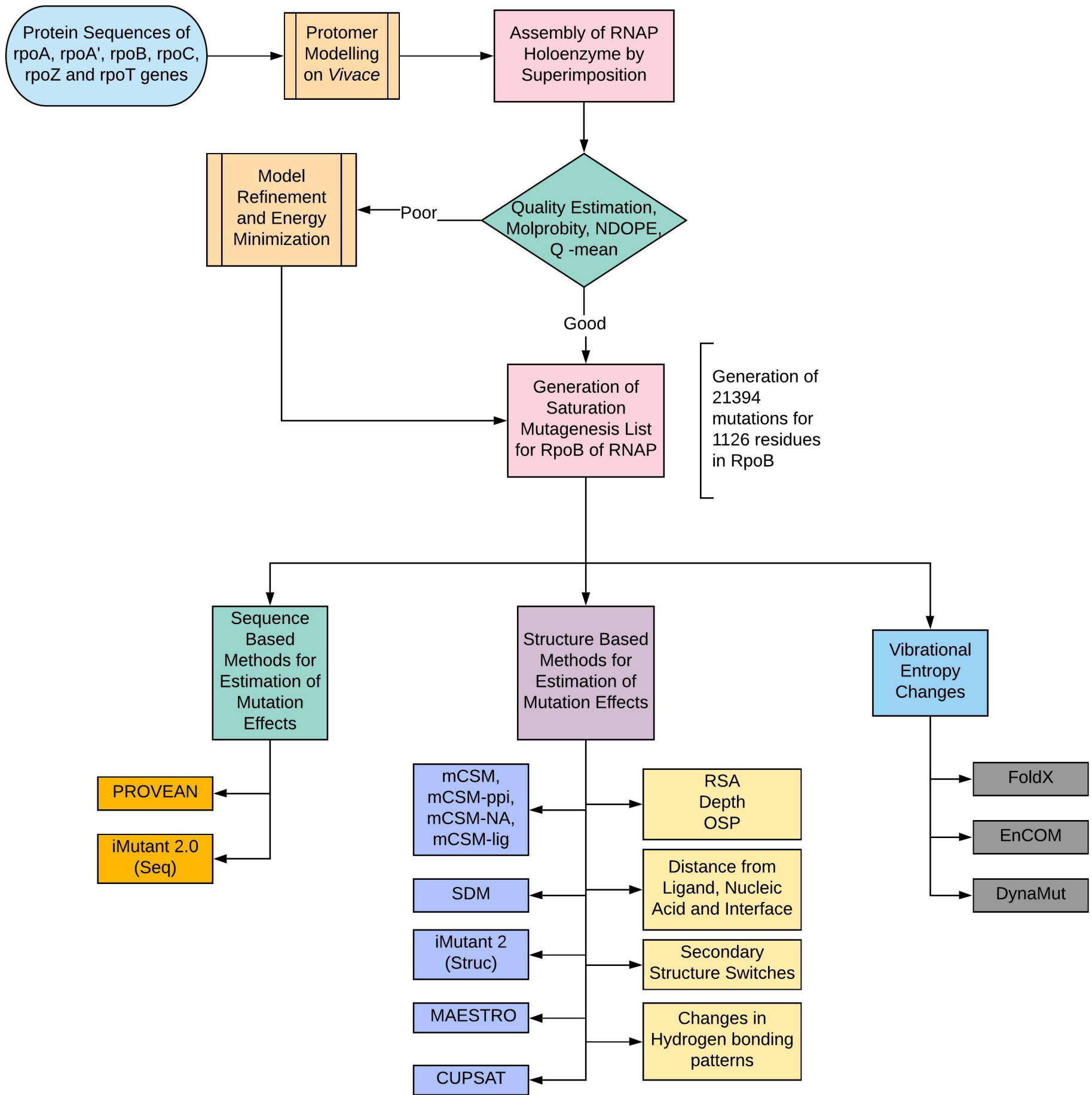
- 568 3. WHO | Weekly Epidemiological Record, 31 August 2018, vol. 93, 35 (pp. 444–456). In:
569 WHO [Internet]. [cited 19 Dec 2018]. Available:
570 <http://www.who.int/wer/2018/wer9335/en/>
- 571 4. Vedithi SC, Malhotra S, Das M, Daniel S, Kishore N, George A, et al. Structural Implications
572 of Mutations Conferring Rifampin Resistance in *Mycobacterium leprae*. *Sci Rep*. 2018;8:
573 5016. doi:10.1038/s41598-018-23423-1
- 574 5. Nakata N, Kai M, Makino M. Mutation Analysis of *Mycobacterium rpoB* Genes and Rifampin
575 Resistance Using Recombinant *Mycobacterium smegmatis*. *Antimicrob Agents Chemother*.
576 2012;56: 2008–2013. doi:10.1128/AAC.05831-11
- 577 6. Pires DEV, Chen J, Blundell TL, Ascher DB. *In silico* functional dissection of saturation
578 mutagenesis: Interpreting the relationship between phenotypes and changes in protein
579 stability, interactions and activity. *Sci Rep*. 2016;6: 19848. doi:10.1038/srep19848
- 580 7. Portelli S, Phelan JE, Ascher DB, Clark TG, Furnham N. Understanding molecular
581 consequences of putative drug resistant mutations in *Mycobacterium tuberculosis*. *Sci*
582 *Rep*. 2018;8: 15356. doi:10.1038/s41598-018-33370-6
- 583 8. Karmakar M, Globan M, Fyfe JAM, Stinear TP, Johnson PDR, Holmes NE, et al. Analysis of a
584 Novel *pncA* Mutation for Susceptibility to Pyrazinamide Therapy. *Am J Respir Crit Care*
585 *Med*. 2018;198: 541–544. doi:10.1164/rccm.201712-2572LE
- 586 9. Ramasoota P, Wongwit W, Sampunachot P, Unnarat K, Ngamyang M, Svenson SB. Multiple
587 mutations in the *rpoB* gene of *Mycobacterium leprae* strains from leprosy patients in
588 Thailand. *Southeast Asian J Trop Med Public Health*. 2000;31: 493–497.
- 589 10. Cambau E, Saunderson P, Matsuoka M, Cole ST, Kai M, Suffys P, et al. Antimicrobial
590 resistance in leprosy: results of the first prospective open survey conducted by a WHO
591 surveillance network for the period 2009–15. *Clin Microbiol Infect Off Publ Eur Soc Clin*
592 *Microbiol Infect Dis*. 2018;24: 1305–1310. doi:10.1016/j.cmi.2018.02.022
- 593 11. Williams DL, Gillis TP. Drug-resistant leprosy: monitoring and current status. *Lepr Rev*.
594 2012;83: 269–281.
- 595 12. Sandgren A, Strong M, Muthukrishnan P, Weiner BK, Church GM, Murray MB. Tuberculosis
596 Drug Resistance Mutation Database. *PLOS Med*. 2009;6: e1000002.
597 doi:10.1371/journal.pmed.1000002
- 598 13. Htike Min PK, Pitaksajakul P, Tipkrua N, Wongwit W, Jintaridh P, Ramasoota P. Novel
599 mutation detection IN *rpoB* OF rifampicin-resistant *Mycobacterium tuberculosis* using
600 pyrosequencing. *Southeast Asian J Trop Med Public Health*. 2014;45: 843–852.
- 601 14. André E, Goeminne L, Colmant A, Beckert P, Niemann S, Delmee M. Novel rapid PCR for the
602 detection of Ile491Phe *rpoB* mutation of *Mycobacterium tuberculosis*, a rifampicin-
603 resistance-conferring mutation undetected by commercial assays. *Clin Microbiol Infect Off*
604 *Publ Eur Soc Clin Microbiol Infect Dis*. 2017;23: 267.e5-267.e7.
605 doi:10.1016/j.cmi.2016.12.009
- 606 15. Al-Mutairi NM, Ahmad S, Mokaddas E, Eldeen HS, Joseph S. Occurrence of disputed *rpoB*
607 mutations among *Mycobacterium tuberculosis* isolates phenotypically susceptible to
608 rifampicin in a country with a low incidence of multidrug-resistant tuberculosis. *BMC*
609 *Infect Dis*. 2019;19: 3. doi:10.1186/s12879-018-3638-z

- 610 16. Lahiri N, Shah RR, Layre E, Young D, Ford C, Murray MB, et al. Rifampin Resistance
611 Mutations Are Associated with Broad Chemical Remodeling of Mycobacterium
612 tuberculosis. *J Biol Chem.* 2016;291: 14248–14256. doi:10.1074/jbc.M116.716704
- 613 17. Andres S, Gröschel MI, Hillemann D, Merker M, Niemann S, Kranzer K. A Diagnostic
614 Algorithm To Investigate Pyrazinamide and Ethambutol Resistance in Rifampin-Resistant
615 Mycobacterium tuberculosis Isolates in a Low-Incidence Setting. *Antimicrob Agents*
616 *Chemother.* 2019;63: e01798-18. doi:10.1128/AAC.01798-18
- 617 18. Schymkowitz J, Borg J, Stricher F, Nys R, Rousseau F, Serrano L. The FoldX web server: an
618 online force field. *Nucleic Acids Res.* 2005;33: W382–W388. doi:10.1093/nar/gki387
- 619 19. Frappier V, Chartier M, Najmanovich RJ. ENCoM server: exploring protein conformational
620 space and the effect of mutations on protein function and stability. *Nucleic Acids Res.*
621 2015;43: W395–W400. doi:10.1093/nar/gkv343
- 622 20. Rodrigues CH, Pires DE, Ascher DB. DynaMut: predicting the impact of mutations on
623 protein conformation, flexibility and stability. *Nucleic Acids Res.* 2018;46: W350–W355.
624 doi:10.1093/nar/gky300
- 625 21. Radoux CJ, Olsson TSG, Pitt WR, Groom CR, Blundell TL. Identifying Interactions that
626 Determine Fragment Binding at Protein Hotspots. *J Med Chem.* 2016;59: 4314–4325.
627 doi:10.1021/acs.jmedchem.5b01980
- 628 22. Davis IW, Murray LW, Richardson JS, Richardson DC. MOLPROBITY: structure validation
629 and all-atom contact analysis for nucleic acids and their complexes. *Nucleic Acids Res.*
630 2004;32: W615-619. doi:10.1093/nar/gkh398
- 631 23. Pettersen EF, Goddard TD, Huang CC, Couch GS, Greenblatt DM, Meng EC, et al. UCSF
632 Chimera--a visualization system for exploratory research and analysis. *J Comput Chem.*
633 2004;25: 1605–1612. doi:10.1002/jcc.20084
- 634 24. Sali A, Blundell TL. Comparative protein modelling by satisfaction of spatial restraints. *J*
635 *Mol Biol.* 1993;234: 779–815. doi:10.1006/jmbi.1993.1626
- 636 25. Smith RE, Lovell SC, Burke DF, Montalvao RW, Blundell TL. Andante: reducing side-chain
637 rotamer search space during comparative modeling using environment-specific
638 substitution probabilities. *Bioinformatics.* 2007;23: 1099–1105.
639 doi:10.1093/bioinformatics/btm073
- 640 26. Ashkenazy H, Abadi S, Martz E, Chay O, Mayrose I, Pupko T, et al. ConSurf 2016: an
641 improved methodology to estimate and visualize evolutionary conservation in
642 macromolecules. *Nucleic Acids Res.* 2016;44: W344-350. doi:10.1093/nar/gkw408
- 643 27. Pires DEV, Ascher DB, Blundell TL. mCSM: predicting the effects of mutations in proteins
644 using graph-based signatures. *Bioinformatics.* 2014;30: 335–342.
645 doi:10.1093/bioinformatics/btt691
- 646 28. Pandurangan AP, Ochoa-Montaño B, Ascher DB, Blundell TL. SDM: a server for predicting
647 effects of mutations on protein stability. *Nucleic Acids Res.* 2017; doi:10.1093/nar/gkx439
- 648 29. Schymkowitz J, Borg J, Stricher F, Nys R, Rousseau F, Serrano L. The FoldX web server: an
649 online force field. *Nucleic Acids Res.* 2005;33: W382-388. doi:10.1093/nar/gki387
- 650 30. Pires DEV, Ascher DB. mCSM-NA: predicting the effects of mutations on protein-nucleic
651 acids interactions. *Nucleic Acids Res.* 2017; doi:10.1093/nar/gkx236

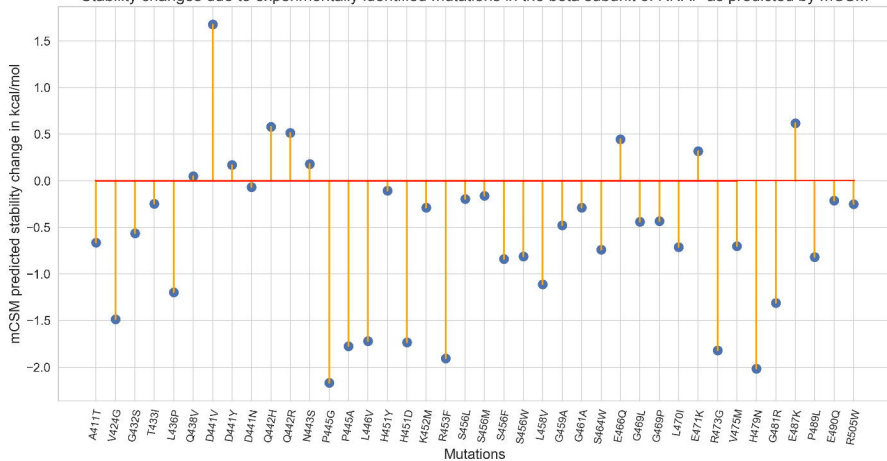
- 652 31. Pires DEV, Blundell TL, Ascher DB. mCSM-lig: quantifying the effects of mutations on
653 protein-small molecule affinity in genetic disease and emergence of drug resistance. Sci
654 Rep. 2016;6: srep29575. doi:10.1038/srep29575
- 655 32. Choi Y, Sims GE, Murphy S, Miller JR, Chan AP. Predicting the Functional Effect of Amino
656 Acid Substitutions and Indels. PLOS ONE. 2012;7: e46688.
657 doi:10.1371/journal.pone.0046688
- 658 33. Capriotti E, Fariselli P, Casadio R. I-Mutant2.0: predicting stability changes upon mutation
659 from the protein sequence or structure. Nucleic Acids Res. 2005;33: W306–W310.
660 doi:10.1093/nar/gki375
- 661 34. Laimer J, Hofer H, Fritz M, Wegenkittl S, Lackner P. MAESTRO - multi agent stability
662 prediction upon point mutations. BMC Bioinformatics. 2015;16: 116. doi:10.1186/s12859-
663 015-0548-6
- 664 35. Parthiban V, Gromiha MM, Schomburg D. CUPSAT: prediction of protein stability upon
665 point mutations. Nucleic Acids Res. 2006;34: W239–W242. doi:10.1093/nar/gkl190
- 666 36. Rodrigues CH, Pires DE, Ascher DB. DynaMut: predicting the impact of mutations on
667 protein conformation, flexibility and stability. Nucleic Acids Res. 2018;46: W350–W355.
668 doi:10.1093/nar/gky300
- 669 37. Jubb HC, Higuero AP, Ochoa-Montaña B, Pitt WR, Ascher DB, Blundell TL. Arpeggio: A
670 Web Server for Calculating and Visualising Interatomic Interactions in Protein Structures. J
671 Mol Biol. 2017;429: 365–371. doi:10.1016/j.jmb.2016.12.004
- 672 38. Strub C, Alies C, Lougarre A, Ladurantie C, Czaplicki J, Fournier D. Mutation of exposed
673 hydrophobic amino acids to arginine to increase protein stability. BMC Biochem. 2004;5: 9.
674 doi:10.1186/1471-2091-5-9
- 675 39. Levy L, Ji B. The mouse foot-pad technique for cultivation of *Mycobacterium leprae*. Lepr
676 Rev. 2006;77: 5–24.
- 677 40. Colston MJ, Hilson GR, Banerjee DK. The “proportional bactericidal test”: a method for
678 assessing bactericidal activity in drugs against *Mycobacterium leprae* in mice. Lepr Rev.
679 1978;49: 7–15.
- 680 41. Comas I, Borrell S, Roetzer A, Rose G, Malla B, Kato-Maeda M, et al. Whole-genome
681 sequencing of rifampicin-resistant *Mycobacterium tuberculosis* strains identifies
682 compensatory mutations in RNA polymerase genes. Nat Genet. 2012;44: 106–110.
683 doi:10.1038/ng.1038
- 684 42. Usmanova DR, Bogatyreva NS, Ariño Bernad J, Eremina AA, Gorshkova AA, Kanevskiy GM,
685 et al. Self-consistency test reveals systematic bias in programs for prediction change of
686 stability upon mutation. Bioinformatics. 2018;34: 3653–3658.
687 doi:10.1093/bioinformatics/bty340
- 688 43. Lin W, Mandal S, Degen D, Liu Y, Ebright Y, Li S, et al. Structural basis of *Mycobacterium*
689 *tuberculosis* transcription and transcription inhibition. bioRxiv. 2017; 099606.
690 doi:10.1101/099606
- 691 44. Boyaci H, Chen J, Lilic M, Palka M, Mooney RA, Landick R, et al. Fidaxomicin jams
692 *Mycobacterium tuberculosis* RNA polymerase motions needed for initiation via RbpA
693 contacts. eLife. 2018;7. doi:10.7554/eLife.34823

694 45. Fischer A, Seitz T, Lochner A, Sterner R, Merkl R, Bocola M. A fast and precise approach for
695 computational saturation mutagenesis and its experimental validation by using an
696 artificial (β)₈-barrel protein. *Chembiochem Eur J Chem Biol.* 2011;12: 1544–1550.
697 doi:10.1002/cbic.201100051


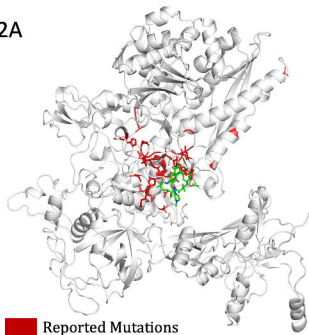
698



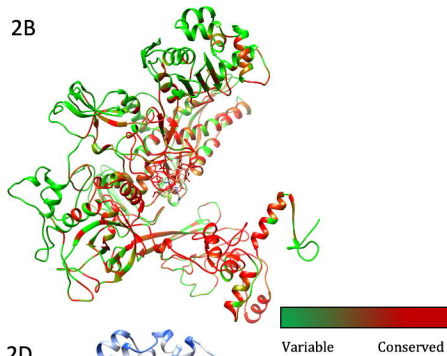
Stability changes due to experimentally identified mutations in the beta subunit of RNAP as predicted by mCSM



2A

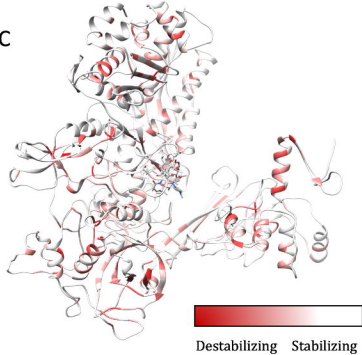
 Reported Mutations

2B



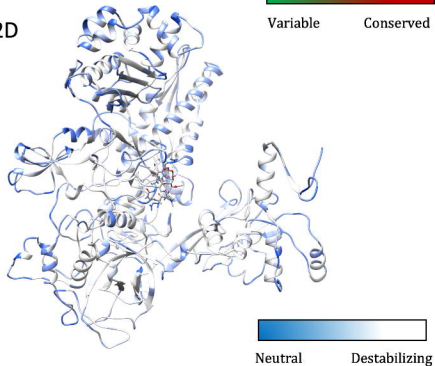
Variable Conserved

2C



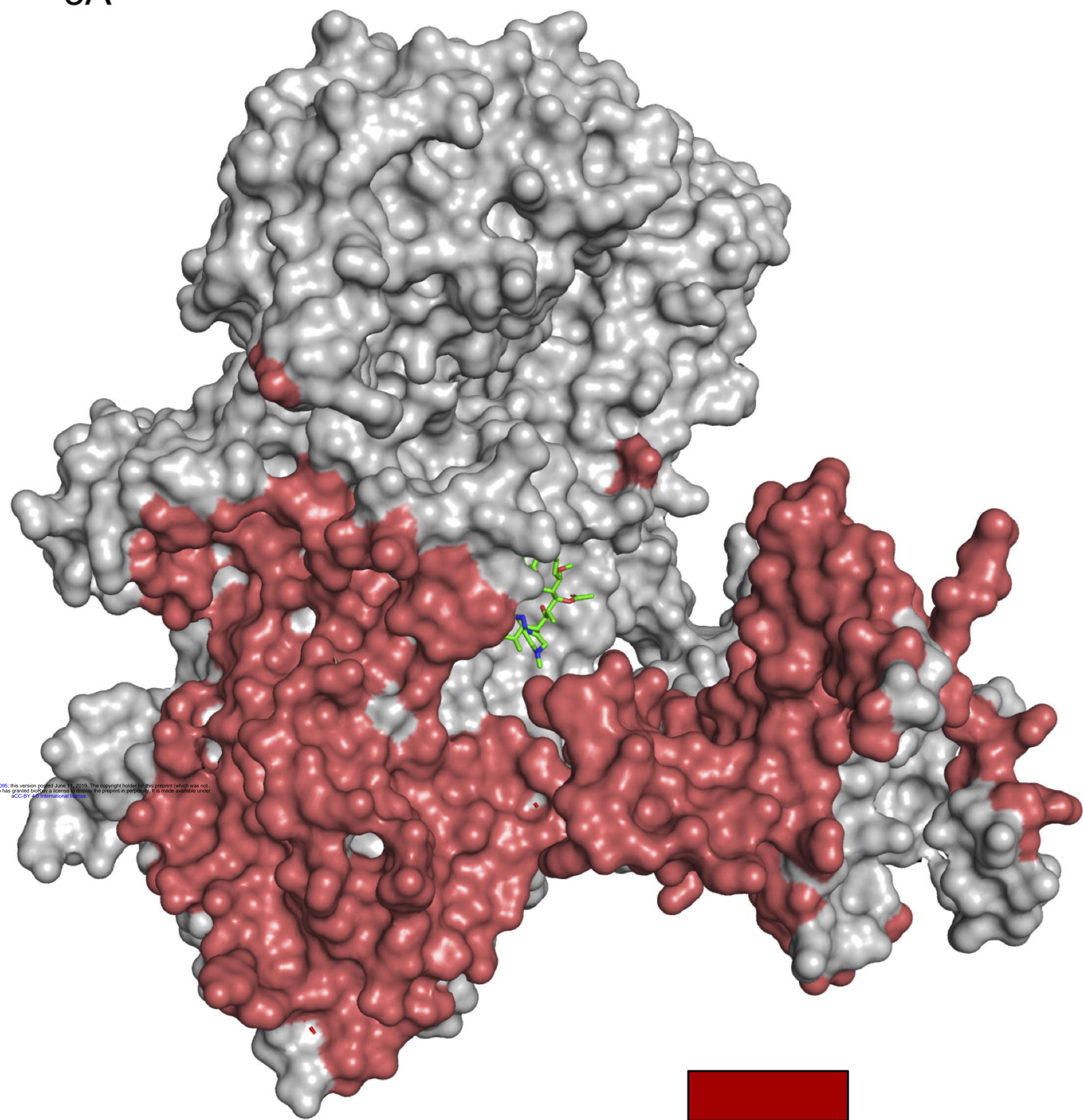
Destabilizing Stabilizing


2D



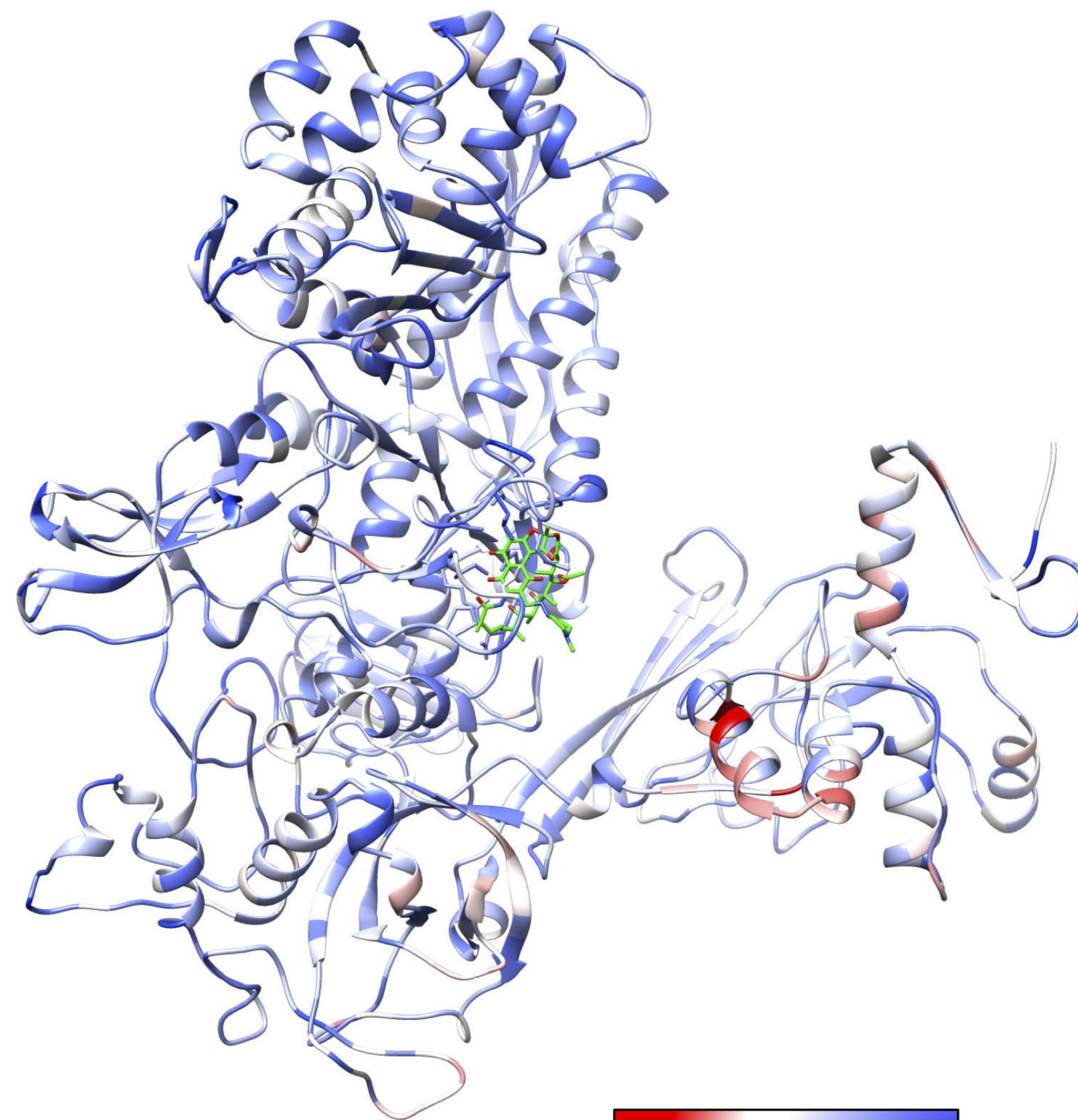
Neutral Destabilizing


3A




Interfacial Region
with β' subunit

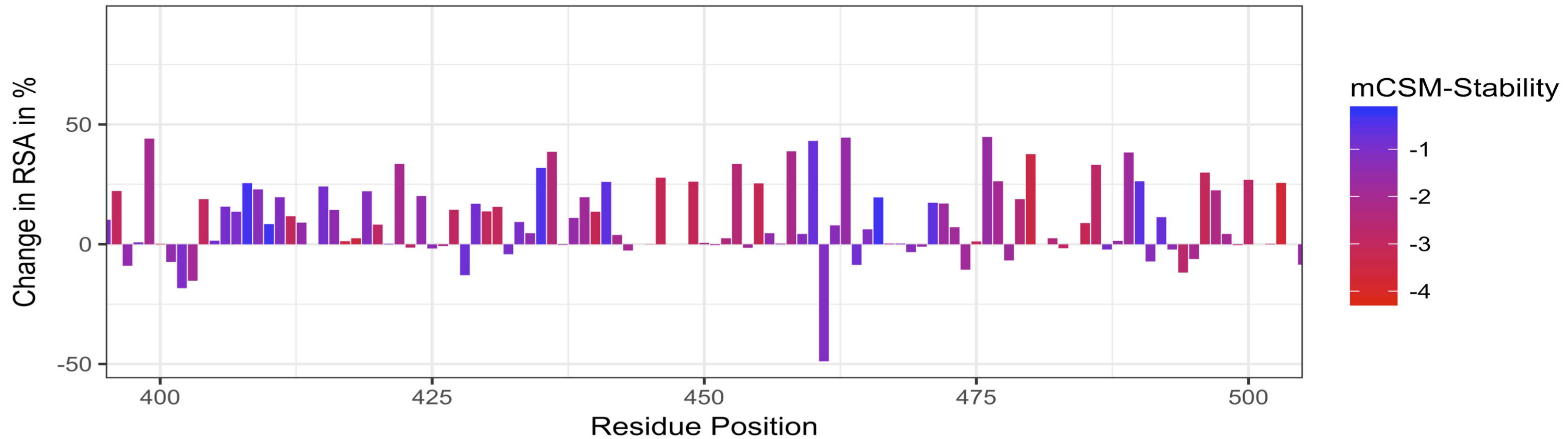
3B




Destabilizing Stabilizing

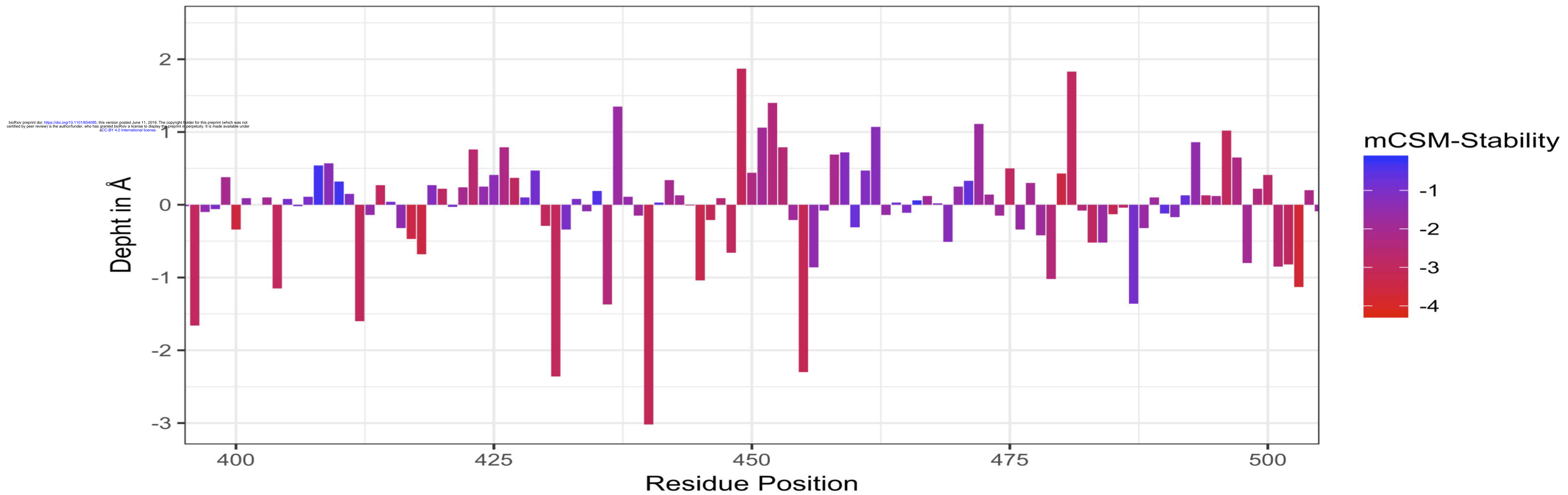
RSA of the Rifampin Binding Site and mCSM-Stability

4A

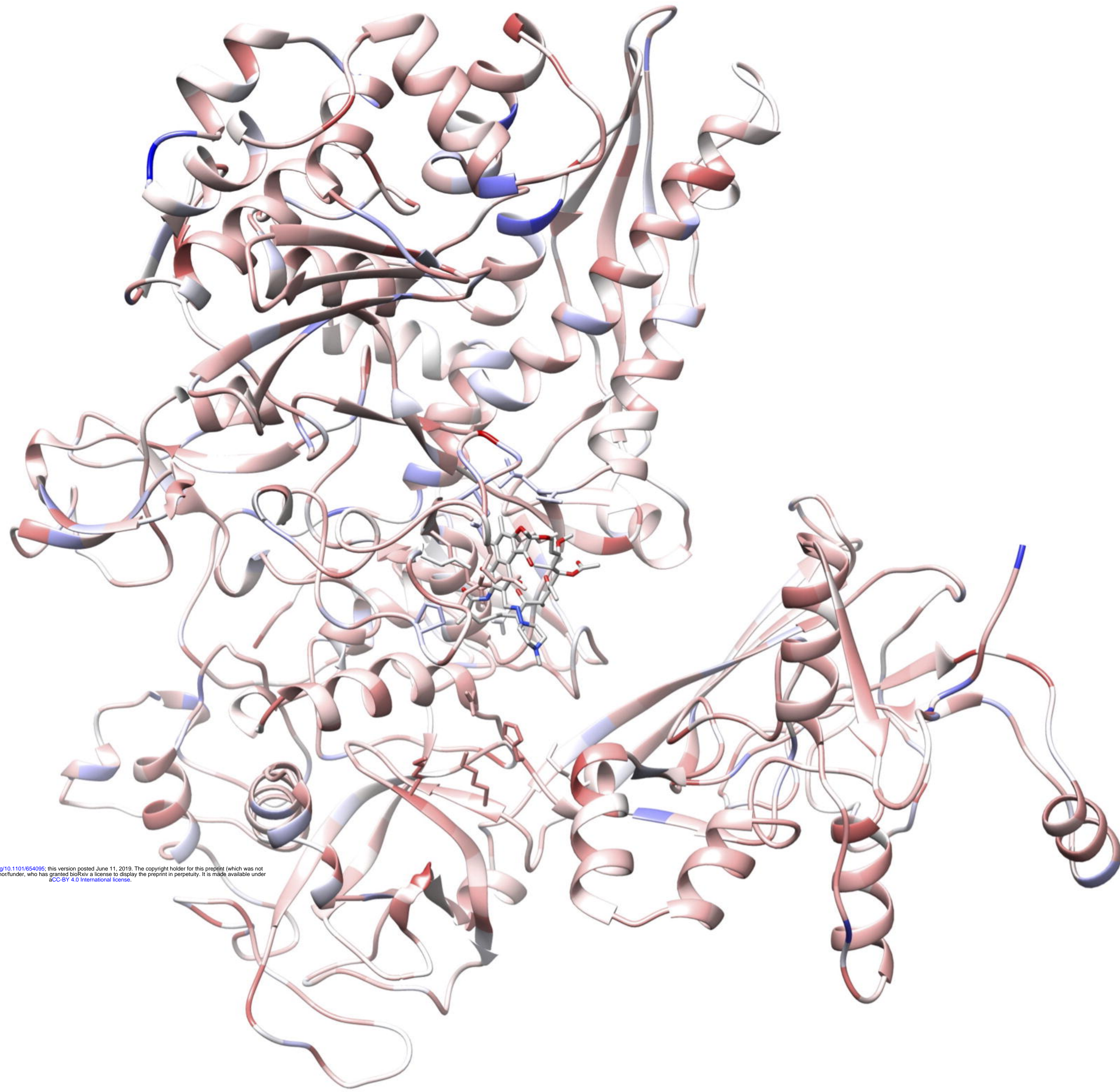


4B

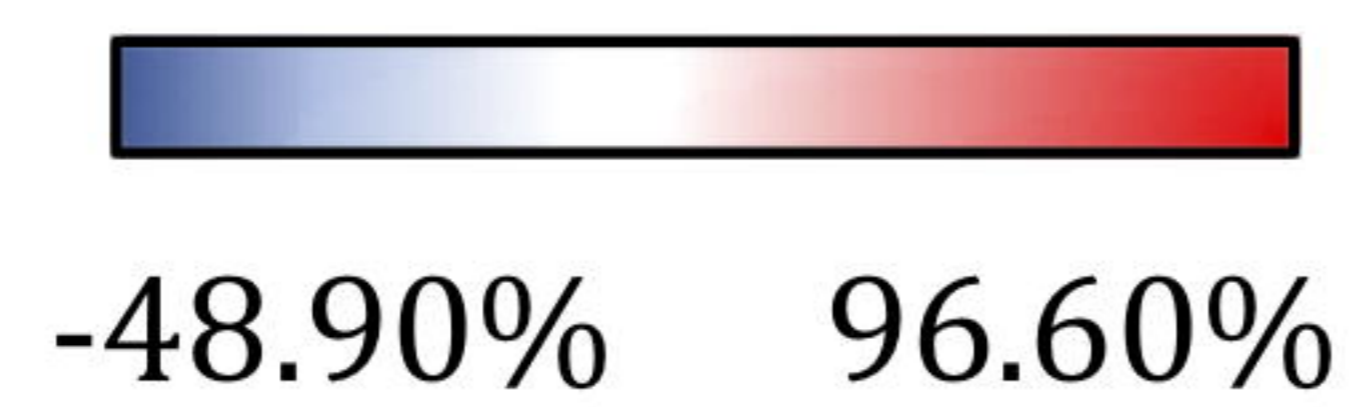
Depth of the Rifampin Binding site and mCSM Stability



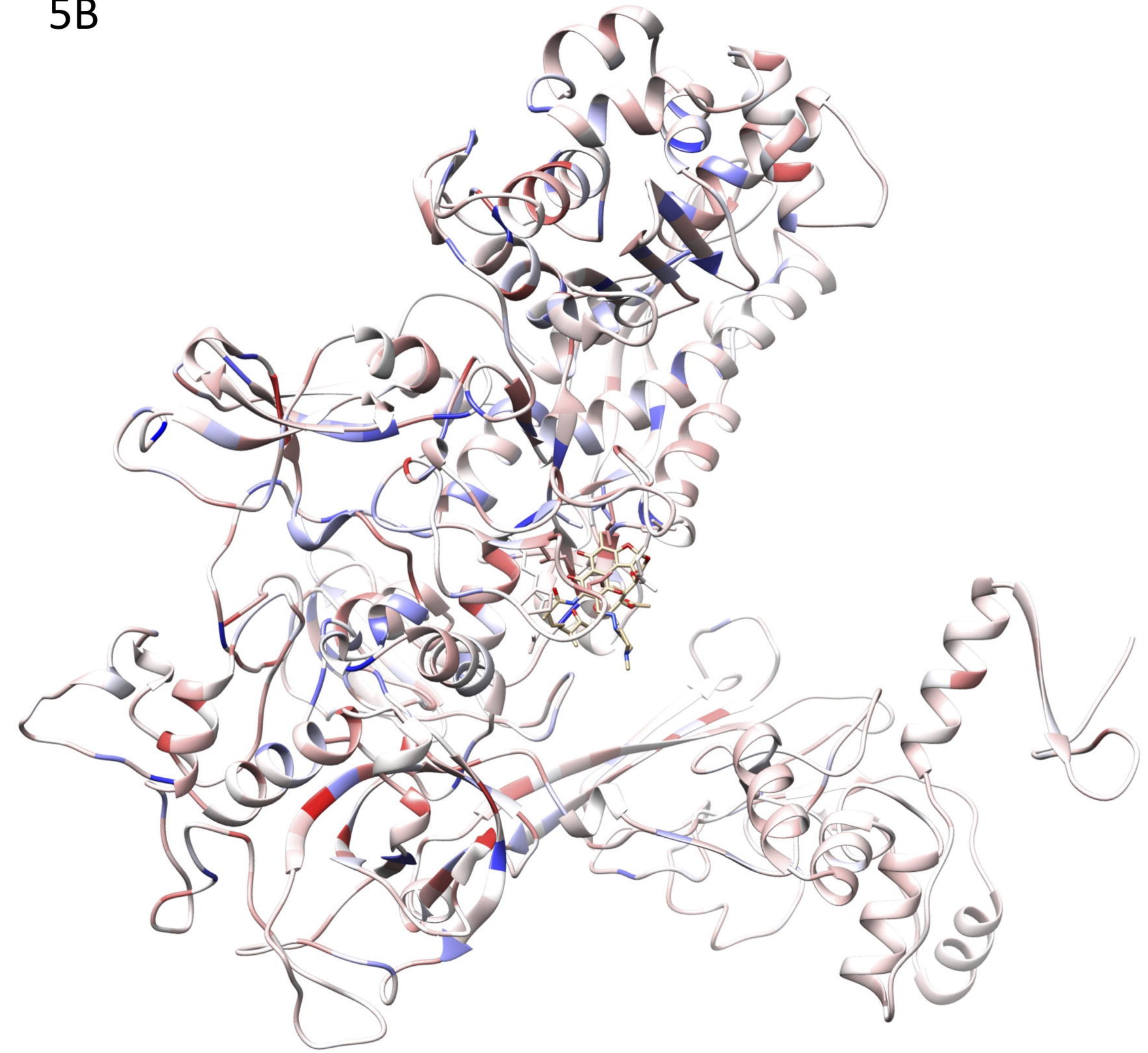
5A



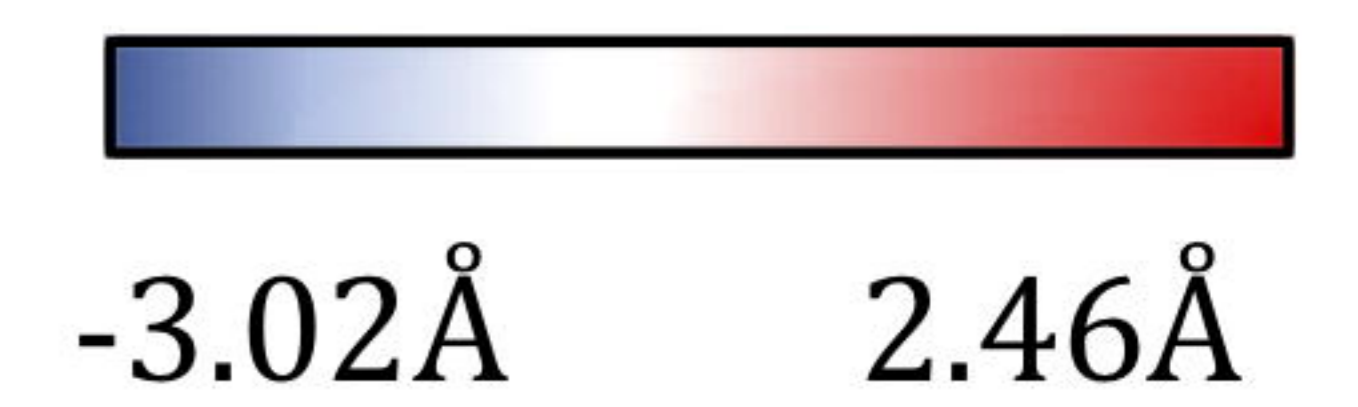
Change in RSA with destabilizing mutations maximum at each residue position.



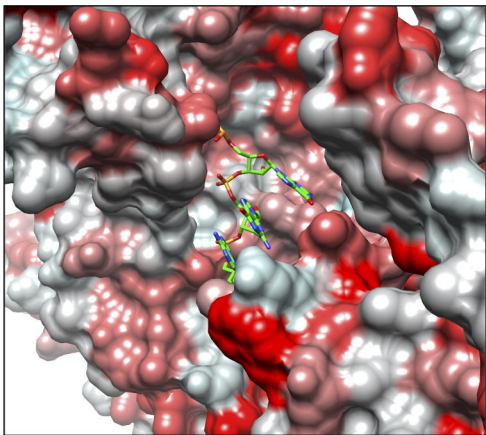
5B



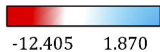
Change in Depth with destabilizing mutations maximum at each residue position.



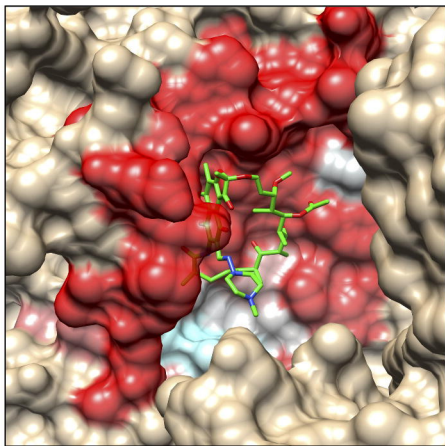
6A



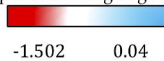
mCSM-NA2 Predictions in the RNA Interacting Region

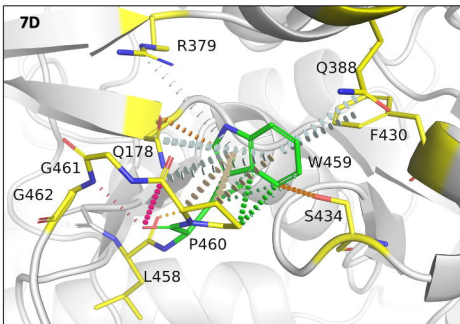
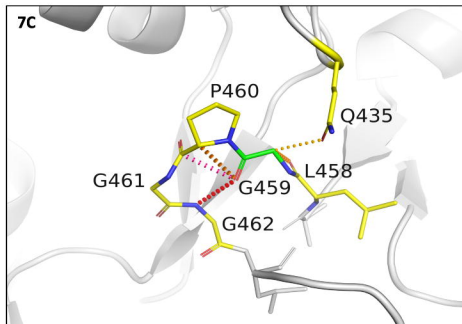
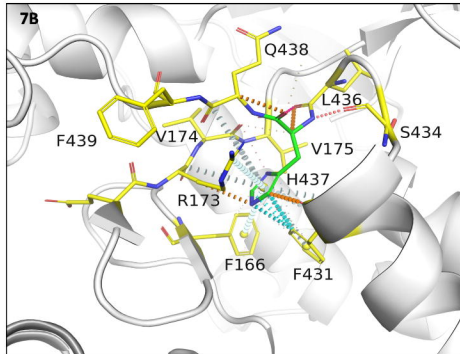
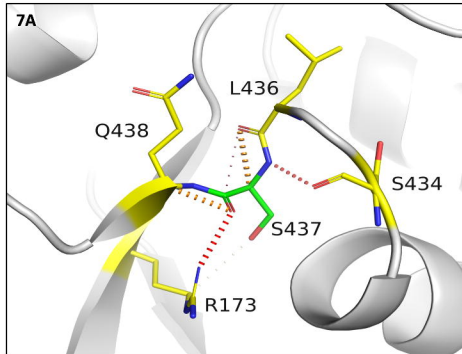


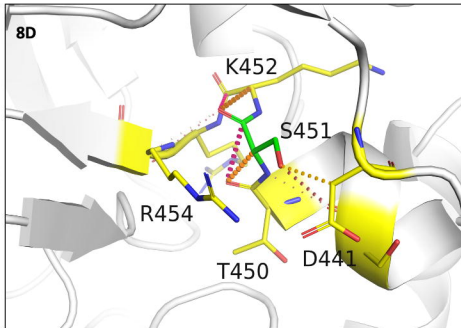
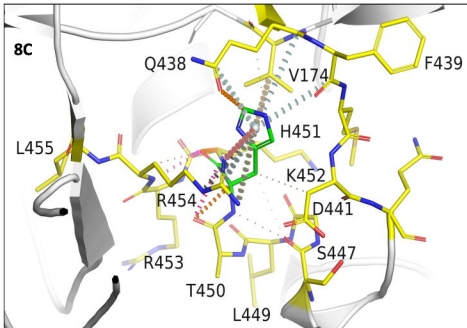
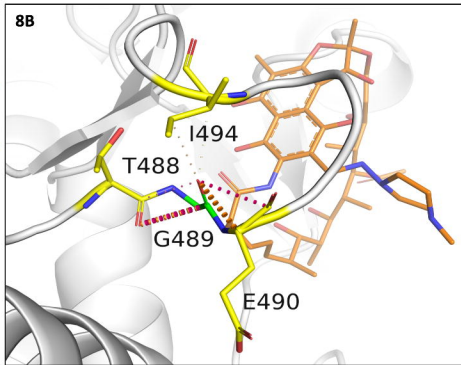
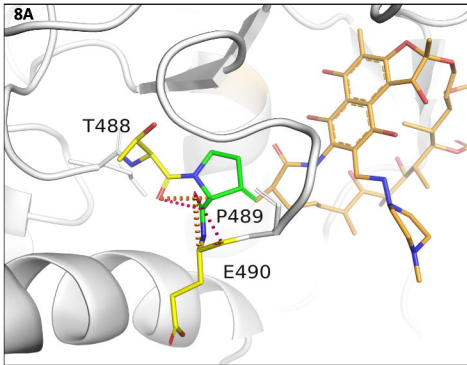
6B

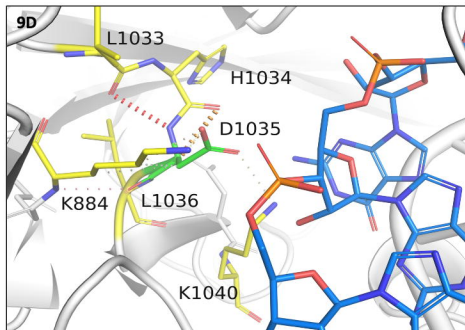
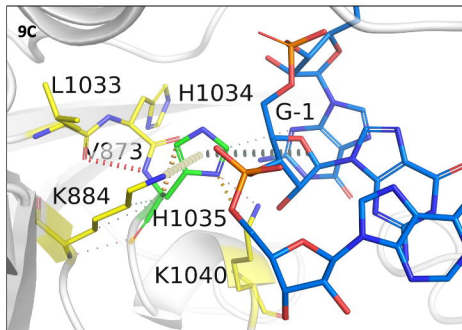
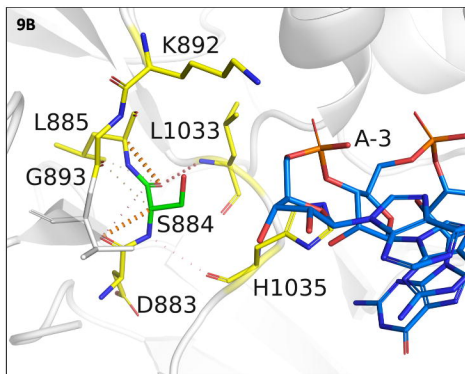
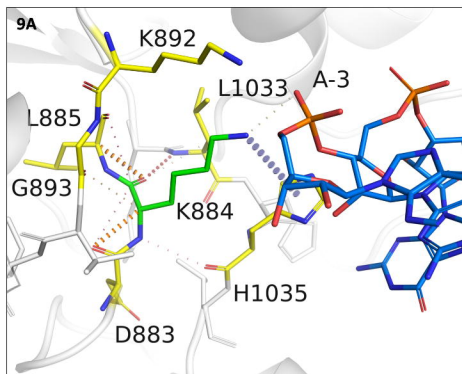


mCSM-Lig Predictions in the Rifampin Interacting Region



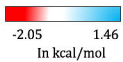




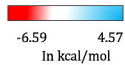
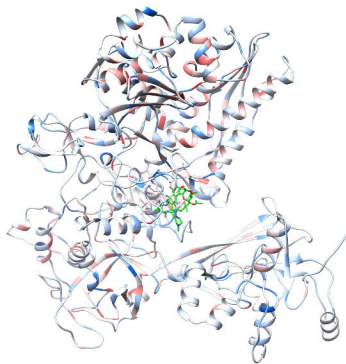


10A

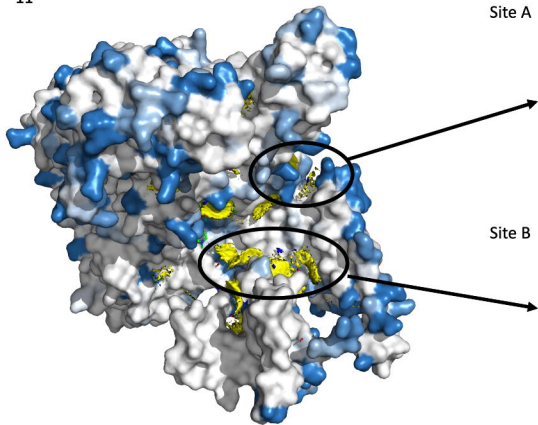
A ribbon diagram of a protein structure, labeled 10A. The protein is shown in a light blue and white color scheme. A green ligand is bound to the protein, located in the center of the structure. The protein is composed of several alpha-helices and beta-sheets.



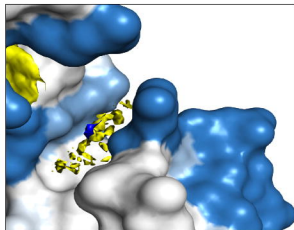
10B



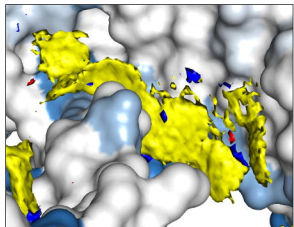
11



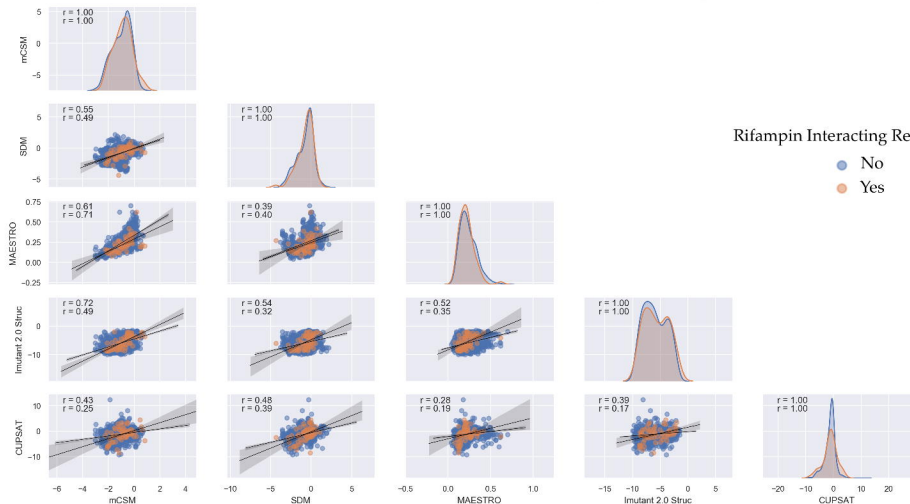
Site A



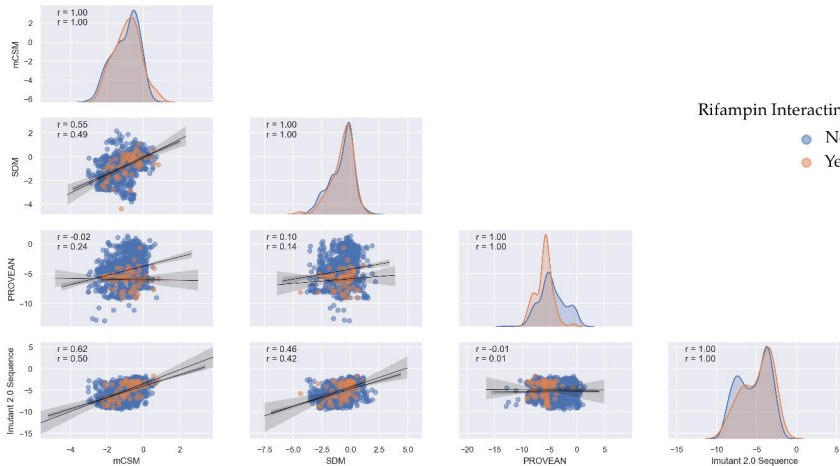
Site B



Correlation between mCSM, SDM and other structure based predictors for protein stability



Correlation between mCSM, SDM and other sequence based predictors for protein stability



Correlation between mCSM, SDM and other Vibrational Entropy Change Predictions

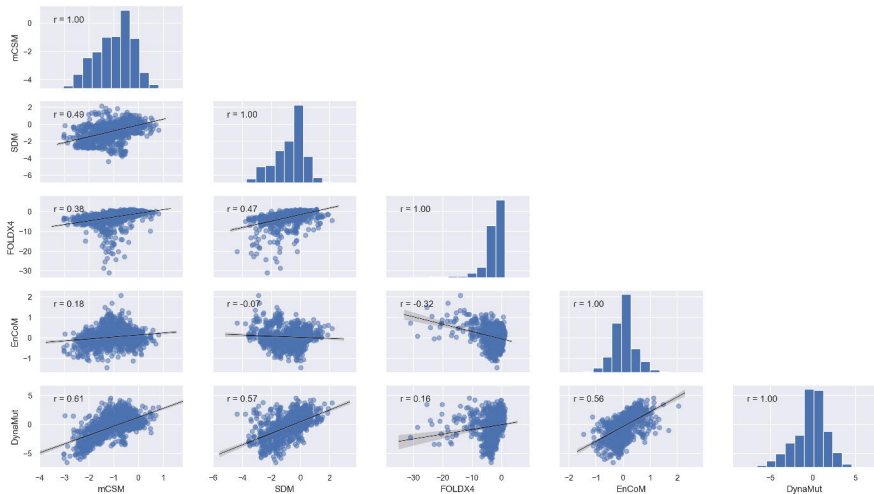


Figure Legends:

Fig 1: [A] Methodology and study design. **[B]** A lollipop plot with stability predictions for mutations reported in literature known to confer rifampin resistance in Leprosy.

Fig 2: [A] The β subunit of RNAP with residues where mutations were reported experimentally from patient samples in various studies (highlighted in red). **[B]** Each residue in the β subunit of RNAP that is colored based on the conservations scores of CONSURF. The residues in green are variable (conservations scores greater than 1) and are usually surface exposed. The residues in red are conserved with conservation scores less than 1 and usually form the core of the protein. The rifampin binding site is highly conserved in *M. leprae*. **[C]** The maximum destabilizing effects (predicted by mCSM) on the protein stability, a mutation can induce at each residue position, is mapped on the structure. Red are the regions that are largely destabilized by mutations while the white regions are relatively stable with mutations. **[D]** The converse of B where the regions that are predicted to be least impact the stability with any mutation are coloured in blue and we called them “Mutation CoolSpots”.

Fig 3: [A] The interfacial region of the β subunit of RNAP highlighted in Maroon. **[B]**. The maximum destabilizing effect a mutation can induce on the interface stability is predicted by mCSM-PPI and mapped on the structure. Red indicates regions that are highly destabilized by mutations (-5.108 Kcal/mol) while the blue indicates stable regions.

Fig 4: [A] Change in relative solvent accessibility for maximum destabilizing mutants in the rifampin binding pocket (mCSM). **[B]**. Change in depth of the highly destabilizing mutant residue in the rifampin binding pocket (mCSM).

Fig 5: [A] The change in relative side chain solvent accessibility with mutations was mapped on to the structure. Blue indicates a decrease in RSA while red indicates an increase. **[B]**The changes in depth with highly destabilizing mutations at each residue position was also mapped on the structure.

Fig 6: [A] Stability changes in β subunit -RNA and β subunit- rifampin [B] interactions due to mutations in the binding sites as predicted by mCSM-NA2 and mCSM-lig. The maximum destabilizing effect a mutation can cause at each residue position in the binding site is depicted on the structure.

Fig 7: [A] Interactions of S437 with the surrounding residue environment in the wildtype and of H437 in the S437H mutant [B]. [C] Interactions of G459 with the surrounding residue environment and [D] W459 in the mutant G459W. The red dotted lines represent hydrogen bonds. Orange dotted lines represent weak hydrogen bond interactions. Ring-Ring and intergroup interactions are depicted in cyan. Aromatic interactions are represented in sky-blue and carbonyl interactions in pink dotted lines. Green dotted lines represent hydrophobic interactions.

Fig 8: [A] Interactions of P489 with the surrounding residue environment in the wildtype and of G489 in the P489G mutant [B]. [C] Interactions of H451 with the surrounding residue environment and [D] S451 in the mutant H451S.

Fig 9: [A] Interactions of K884 with the surrounding residue environment in the wildtype and of S884 in the K884S mutant [B]. [C] Interactions of H1035 with the surrounding residue environment and [D] D1035 in the mutant H1035D. The blue dotted lines represent cation- π interaction.

Fig 10: [A] The maximum destabilizing effects on the protein stability, a mutation can induce at each residue position in the flexible conformations (as predicted by ENCoM [A] and DynaMut [B]), are mapped on the structure. Regions in red represent highly destabilizing while the blue regions are relatively stable with mutations.

Fig 11: Fragment hotspots were mapped on the structure which was coloured with maximum destabilizing effects of systematic mutations at each residue positions. Blue represents regions which are least impacted by any mutations. Stable and potential small molecule binding sites "A" and "B" are depicted on the structure.

Supplementary Figure 1: Pairplot depicting correlations between mCSM, SDM and other structural predictors of protein stability changes upon mutations in the β subunit of RNAP. Each datapoint corresponds to maximum destabilizing effect noted at each residue position in the β subunit when systematically mutated to other 19 residues. The data points in orange correspond to predictions at rifampin interacting residues.

Supplementary Figure 2: Pairplot depicting correlations between mCSM, SDM and other sequence-based predictors of protein stability changes upon mutations in the β subunit of RNAP. Each data point corresponds to maximum destabilizing effect noted at each residue position in the β subunit when systematically mutated to other 19 residues. The data points in orange correspond to predictions at rifampin interacting residues.

Supplementary Figure 3: Pairplot depicting correlations between mCSM, SDM and other NMA-based predictors of protein stability changes upon mutations in the β subunit of RNAP. Each data point corresponds to average destabilizing effect noted at each residue position in the β subunit when systematically mutated to other 19 residues.